Doctoral Thesis

Photo/electro-stimulated Charge Transfer in Triboelectric Nanogenerator

Byeong Uk Ye

Department of Materials Science and Engineering

Graduate School of UNIST

2017

Photo/electro-stimulated Charge Transfer in Triboelectric Nanogenerator

Byeong Uk Ye

Department of Materials Science and Engineering

Graduate School of UNIST

Photo/electro-stimulated Charge Transfer in Triboelectric Nanogenerator

A thesis/dissertation
submitted to the Graduate School of UNIST
in partial fulfillment of the
requirements for the degree of
Doctor of Philosophy

Byeong Uk Ye

12. 15. 2016
Approved by

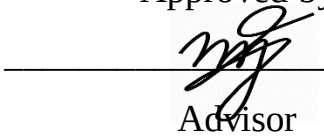

Advisor
Jeong Min Baik

Photo/electro-stimulated Charge Transfer in Triboelectric Nanogenerator

Byeong Uk Ye

This certifies that the thesis/dissertation of Byeong Uk Ye is approved.

12. 15. 2016

signature

Advisor: Jeong Min Baik

signature

Kyoung Jin Choi: Thesis Committee Member #1

signature

Chong-Yun Kang: Thesis Committee Member #2

signature

Myoung Hoon Song: Thesis Committee Member #3

signature

Soon-Yong Kwon: Thesis Committee Member #4;

Abstract

Widespread energy harvesting, generating self-sufficient power from the surrounding environment, such as wind, solar and geothermal, have attracted increasing attention in the past decade due to the energy crisis and global warming. Among them, many technological devices converting mechanical energy into other forms of energy or vice versa have been proposed and investigated because of an extended life time, no recharging procedures, and their scalability. Generally, mechanical energy converted into electricity, namely, by using electromagnetic, electrostatic, and piezoelectric effects. Most recently, a new type of power generating device, named as triboelectric nanogenerator (TENG) based on triboelectric effects coupled with electrostatic effects have been demonstrated as powerful means of harvesting mechanical energy from living environment.

Part 1. A simple fabrication route for ion gel nanofibers in a triboelectric nanogenerator was demonstrated. Using an electrospinning technique, we could fabricate a large-area ion gel nanofiber mat. The triboelectric nanogenerator was demonstrated by employing an ion gel nanofiber and the device exhibited an output power of 0.37 mW and good stability under continuous operation.

Part 2. Understanding the charge transfer mechanism between two surfaces during the physical contact is crucial in the development of triboelectrification-related commercialized products. Here, we report that light illumination can reverse the direction of the charge transfer and significantly increase tribo-charge density occurring at the oxide/polyimide interface. Under light illumination, the surface potential maps of TiO_x layer on P3HT:PC_{61}BM/PEDOT:PSS/ITO substrate showed the significant decrease of the work function by approximately 0.2 eV, positioned to be at lower than that of the polyimide and thus increasing the work function difference with the polyimide. The wavelength-dependent

measurement of the output open-circuit voltages revealed that the photogenerated electrons from active layer via visible light were accumulated at the surface of TiO_x, enhancing the output short-circuit current of the triboelectric nanogenerator by 5 times, supported by the gate voltage-dependent output performance of the nanogenerator with $TiO_x/SiO_2/Si$ substrate connected to the back gate metal. These results should help design improved energy harvesting devices as well as self-powered selective wavelength photodetectors.

Contents

LIST OF FIGURES

appeared peaks at 1152, 796, and 613 cm^{-1} are related to the α-phase of P(VDF-HFP). Several peaks in the region between 1348, 1132, 500 and 750 cm^{-1} are assigned to [EMIM][TFSI] related peaks.

Figure 7. (a) Output open-circuit voltage and (b) short-circuit current density of the TENG composed of spin coated P(VDF-HFP) film and electrospun nanofibers. The active area of device was 1 cm × 1 cm. (c-d) Electrical output performance of the ion gel nanofibers based TENG with various ionic liquid doping concentrations (0-10 wt%) under same mechanical force (90 N).

Figure 8. Output open-circuit voltage characteristics of TENGs with various polymer nanofibers as triboelectric materials. All polymer nanofibers were fabricated using an electrospinning process. (a) PVDF, (b) PVP, (c) PS, (d) PMMA.

Figure 9. Output open-circuit voltage signal of TENG under the (a-b) forward and (c-d) reverse connections.

Figure 10. Schematic diagram of electric power generation process of (a-c) bare P(VDF-HFP) and (d-f) ion gel based triboelectric nanogenerators.

Figure 11. (a) Output open-circuit voltage and (b) short-circuit current characteristics of TENG with 20 wt% ion gel nanofibers.

Figure 12. Operational stability of ion gel based TENG. (a) open-circuit voltage and (b) short-circuit current density characteristics of a TENG operated continuously for 10,000 cycles, acquired at f = 5 Hz. (c) Change of output open-circuit voltage of a TENG as a function of operating cycle. Inset: Change of short-circuit current for a TENG and SEM images (100 μm × 100 μm) of ion gel nanofibers (10 wt%) surface before and after 10,000 cyclic operation. (d) A snapshot of the 15-LEDs

arrays lit up by the power output generated from the TENG.

Figure 13. Schematic diagram of the photovoltaic structured triboelectric nanogenerator. (a) schematic illustration for the fabrication process of triboelectric nanogenerator. (b) a photo of triboelectric nanogenerator. (c), (d) cross-sectional and top view (TiO_x) SEM images. (e) the absorption spectra of TiO_x/P3HT:PC_{61}BM/PEDOT:PSS/ITO and TiOx/ITO layers. (f) the output short-circuit current of the triboelectric nanogenerator with the measuring time under dark condition. (g) the expanded view of the output short-circuit current.

Figure 14. (a) The fabrication process of organic photovoltaic cells with Al/TiO_x/P3HT:PC_{61}BM/PEDOT:PSS/ITO/glass. (b) The current-density versus voltage (J–V) characteristics with and without TiO_x layer. (c) The energy band diagrams for Al/TiO_x/P3HT:PC_{61}BM/PEDOT:PSS/ITO/glass under light illumination.

Figure 15. Electrical outputs of triboelectric nanogenerator. (a) the output short-circuit current of the triboelectric nanogenerator under dark condition and white light illumination. (b) the charge density measured under same condition.

Figure 16. TiO_x layer work function variation before and after the light exposure. (a) the schematic illustration of KPFM measurement under dark condition and light illumination. (b) Topography and (c) surface potential maps of TiO_x layer on P3HT:PC_{61}BM/PEDOT:PSS/ITO substrate of same region with the light illumination.

Figure 17. Effect of electron accumulation on output performance in TiO_x layer. (a) the schematic picture and a photo of gated triboelectric nanogenerator consisting of

CHAPTER 1. INTRODUCTION

An ionic liquid that consists of low molar mass cations and anions has attracted great attention in charge transport and in electrochemical experiments. To improve the processability of an ionic liquid for use in practical devices, it is desirable to blend ionic liquids with network-forming block copolymers, and the resulting materials are referred to as “ion gels”. Ion gels have been shown to have exceptional physical properties, such as a high ionic conductivity, short polarization time, good thermal stability, and outstanding mechanical strength. As a result, ion gel is a promising material for use as an electrolyte for batteries, supercapacitors, organic/inorganic transistors, and electrochromic displays. Recently, the functionality of ion gels has been expanded to include flexible electrochemiluminescence. In most cases, ion gels are processed by spin coating or by direct write printing, and thus, they have either only bulk or 2D thin-film structures that, when compared to nano-wire/nano-dots structures, have a relatively small surface area and a limited functionality. Thus, even though there has been an increase in the amount of attention in various research fields on ion gels, its applications have been limited to electrolyte materials in battery/capacitors and in gate insulating materials in transistors. To the best of our knowledge, there has been no report on the formation of electrospun ion gels with a nanofiber structure and on their application for active materials in energy harvesting devices.

Various kinds of nanogenerators have been reported, and of these, the triboelectric nanogenerators (TENG) have attracted much attention. The operation principle of a TENG is based on coupling with an electrostatic effect, resulting in high energy efficiency, simplicity, and scalability. Thus, these have been implemented in power sources for electroplating, UV-detection, health care device, and chemical sensors. The physical properties of triboelectric materials, such as their surface roughness, electron affinity, friction and capacitance, affect the

performance of TENG, and a high capacitance is required to improve the output performance of the devices in term of the output open-circuit voltage and short-circuit current. Ion gel had been previously reported to be able to form an electrical double layer with a very high capacitance (> 10 $\mu F/cm^2$) by an externally applied bias. In addition, the ion gel capacitance is independent of its thickness, implying that we can control the thickness of the triboelectric material in TENG from the nano to the micrometer scale. Thus, ion gels can be applied as triboelectric materials in TENG and can improve the energy conversion efficiency of the devices.

Contact electrification is a well-known phenomenon occurring when two objects get in touch each other, i.e. the objects become spontaneously and oppositely charged due to the charge transfer between them, which intrinsically depends on the intrinsic properties of the objects according to the triboelectric series. The contact electrification phenomenon has allowed the construction of frictional electrostatic generators such as Van de Graaff generator, Lorentz generator, and Holtz machine, but it was also fully utilized in many applications such as chemical sensors, electrostatic charge patterning, and laser printing. Recently, triboelectric nanogenerator (TENG) coupled with electrostatic effect was proposed as new energy generating device. Many possible applications such as environmental/infrastructure monitoring, wearable devices, implantable devices, charging portable electronics and self-powered sensors (i.e. pressure, motion, acoustic sensor) are successfully demonstrated so far. Although there are still many issues to be solved, some technologies are good enough to reach commercialization.

Although the charge transfer has been studied so long, the rapid development of new nanomaterials and the wide potential applications of the triboelectrification-based technologies increased the needs to enhance the fundamental understanding of the phenomena due to the complex interaction between many factors affecting the charge transfer. In general, the generated

potential between two objects was known to be determined by the density of charges transferred. The charge density significantly depends on the physical and chemical properties of the materials as well as many environmental factors (i.e. relative humidity, temperature, and pressure). The probability of the charge transfer is determined by the band alignment of two different materials, thus, control over the work function is the key to increasing the charge density. Various surface modifications technologies such as plasma treatments, self-assembled monolayers, aligned dipole moment etc., were applied to control the surface potential and were proven to be so effective. Light-induced surface potential change was also reported to be quite useful in fabricating photodetectors based on the triboelectrification. However, most of the works have focused on the triboelectric negative materials except of extremely few papers. Furthermore, there was no report on the increase of the surface charge density by the light illumination.

CHAPTER 2. THEORETICAL BACKGROUND

2.2 Triboelectricity

Triboelectricity is characterized by a number of regularities. When friction occurs between two chemically identical bodies, the denser body is positively charged. When there is friction between a metal and a dielectric, the metal may be electrified with either positive or negative polarity. When friction occurs between two dielectrics, the dielectric with the higher dielectric constant e is positively charged. Triboelectricity in solids is attributed to the transfer of charge carriers from one body to the other. In the cases of two metals, two semiconductors, or a metal and a semiconductor, triboelectricity is caused by the transfer of electrons from the substance with the lower work function to the substance with the higher work function. When two different materials are brought into contact and separated, an electric charge is transferred from one to the other.

Positive			Negative
	Polyformaldehyde 1.3-1.4	(continued)	
	Etylcellulose	Polyester (Dacron)	
	Polyamide 11	Polyisobutylene	
	Polyamide 6-6	Polyuretane flexible sponge	
	Melanime formol	Polyethylene Terephthalate	
	Wool, knitted	Polyvinyl butyral	
	Silk, woven	Polychlorobutadiene	
	Aluminum	Natural rubber	
	paper	Polyacrilonitrile	
	Cotton, woven	Acrylonitrile-vinyl chloride	
	Steel	Polybisphenol carbonate	
	Wood	Polychloroether	
	Hard rubber	Polyvinylidine chloride (Saran)	
	Nickel, copper	Polystyrene	
	Sulfur	Polyethylene	
	Brass, silver	Polypropylene	
	Acetate, Rayon	Polyimide (Kapton)	
	Polymethyl methacrylate (Lucite)	Polyvinyl Chloride (PVC)	
	Polyvinyl alcohol	Polydimethylsiloxane (PDMS)	
	(continued)	Polytetrafluoroethylene (Teflon)	

Figure 1. Triboelectric series of various materials.

2.2.1 Effect of the work function on electron transfer

Charge generated by triboelectrification between materials in contact and separation is a prime cause of triboelectricity. The charge transfer is explained in terms of 'electron transfer' arising from the difference in work function between the surfaces. If two metals of different work functions are placed in contact, the Fermi levels of the two metals will coincide and this will result in a potential difference being established between the adjacent faces of the two samples. Two metals with different work functions ϕ_1 and ϕ_2 in contact are schematically shown in Figure 2. Assuming that electron transfer takes place by tunneling so that thermodynamic equilibrium prevails, the contact potential difference V_c is given by

$$V_c = V_{1/2} = -\frac{(\emptyset_1 - \emptyset_2)}{e}$$

where $V_{1/2}$ is the contact potential difference of metal 1 against metal 2, e is the elementary charge. The amount of the transferred charge is equal to the product of the contact potential difference and the capacitance between the two bodies. The capacitance depends on the state of the contacting surfaces. Although the position of the electrons can vary after the metals are separated, the net charge transferred Δq_c is approximated by the following equation:

$$\Delta q_c = C_0 V_c$$

where C_0 is the capacitance between the bodies at the critical separation distance where the charge transfer is cutoff. The difference is probably caused by uncertain factors, such as surface roughness, impurities, oxidized layer, separation speed, and others.

When the insulators come to contact, electrons move from the filled surface states of insulator 1 to the empty surface states of insulator 2. The driving force for the charge transfer between the surfaces is the difference in the effective work functions of the two surfaces.

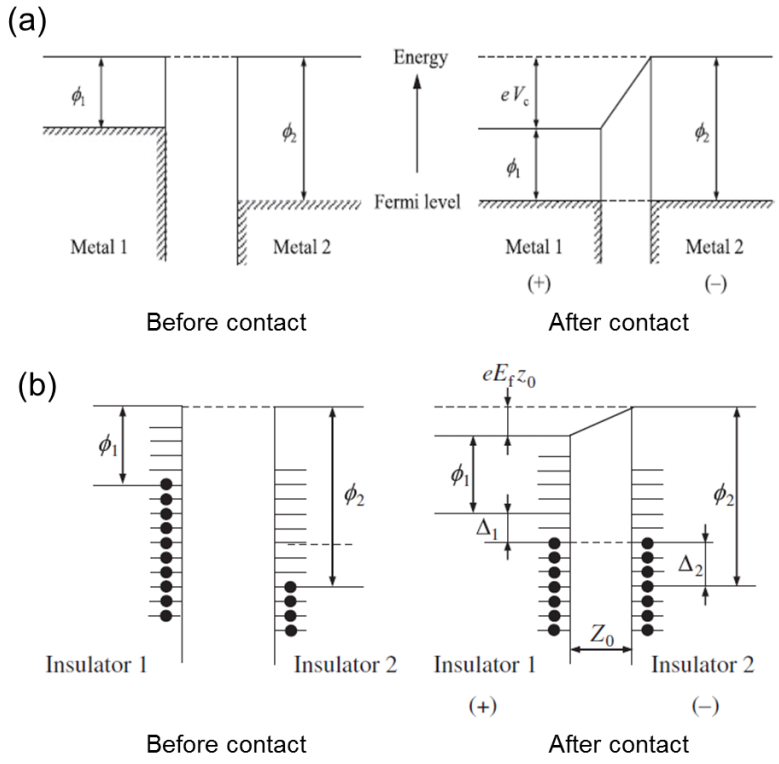

Figure 2. Electron potential energy. (a) metal–metal contact and (b) insulator-insulator contact.

2.2.2 Triboelectric energy harvesting

Energy is one of the most important resources that determines the quality of human life. With the limited fossil energy available for the next century, the search for alternative energy sources remains one of the most important ongoing endeavors of our age. So far, the most favorable energy sources have been considered to be solar, the wind, and tidal energy. Such energy sources have contributed to the major power grids to meet the needs of mega- to gigawatt power scales. The general requirements for harvesting these types of energies are low-cost, high stability, and high efficiency.

In the last two decades, the vast applications and distributions of mobile electronics have reached every corner of our life. Vast types of sensors for health monitoring, medical care,

environmental protection, infrastructure monitoring and security have been developed. The power for driving each unit is small and can be down to million to micro-watt range, but the number of units can be huge. As predicted by Cisco, by 2020 the world will have trillions of sensor units distributed on the earth.1 The recent development of internet of things (IoT) and sensor networks dramatically change the traditional understanding about energy. The general characteristics of these types of power units are mobility, availability, and sustainability. The most conventional technology is using batteries, which may not be the solution for IoT. For trillions of batteries that are vastly distributed and each having a limited lifetime, monitoring, replacing, recycling and exchanging batteries would be a huge and even an impossible task. Most of the IoT would be impossible without making the devices self-powered. It is thus desirable to integrate an energy harvester together with a battery to form a self-powered system and it is likely to be an ideal choice. This was the background for the birth of triboelectric nanogenerators, a revolutionary approach toward nanoenergy.

In the triboelectric process, energy conversion is achieved by a periodic physical contact between two materials that differ in the polarity of triboelectricity, which yields surface charge transfer. The subsequent separation of the two charged materials induces an electronic potential difference, driving the flow of electrons through an external load. In traditional TENGs, the two materials were chosen according to the difference in surface potentials, e.g., the polymer material (i.e. Teflon) terminated with the most electronegative functional group as the negative side and the low work function material (i.e. Al metal) as the positive side, apart from each other (named as airgap). When the two materials are contacted, the polymer material at the negative side tends to gain electrons from Al metal, resulting in being negative compared with Al. Thus, a key approach to improve the output performance of the TENGs from the materials aspect is to increase the triboelectric surface charge density through material modification and surface functionalization. So far, interesting material modifications such as the dielectric constant, the

compressibility, and the surface potential, in a few types of TENG have been reported. However, the density of surface charges was primary determined by the intrinsic properties of the specific materials and there are no effective ways to enhance the output power of TENGs.

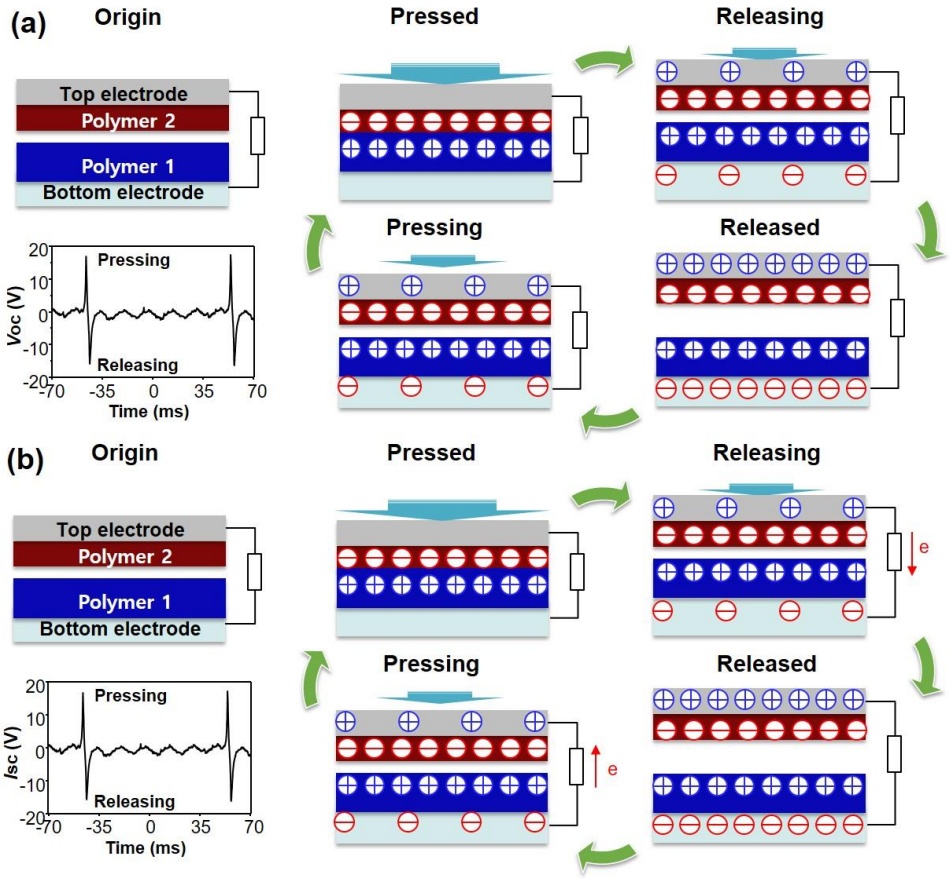

Figure 3. Schematic diagrams that illustrate the operating principle of the generator. (a) Open-circuit condition. (b) Short-circuit condition.

Figures 3a and 3b shows the electric output of open-circuit voltage and short-circuit current. In the original state, no charge is generated or induced, with no electric potential difference (EPD) between the two electrodes. With an externally applied force, the two polymers are brought into contact with each other. Surface charge transfer then takes place at the contact area due to triboelectrification. According to the triboelectric series, which is a list

of materials based on their tendency to gain or lose charges, electrons are injected from polymer 1 into polymer 2, resulting in net negative charges at the polymer 2 surface and net positive charges at the polymer 1 surface, respectively. It is worth noting that the insulating property of the polymers allows a long-time retention of triboelectric charges for hours or even days. Since they are only confined on the surface, charges with opposite signs coincide at almost the same plane, generating practically no EPD between the two electrodes.

CHAPTER 3. EXPERIMENTAL PROCEDURE

3.1 Electrostimulated triboelectric generation

Preparation of the ion gel solution: poly(vinylidene fluoride-co-hexafluoropropylene), P(VDF-HFP) with M_n = 130 000 g mol^{-1} and Mw = 400 000 g mol^{-1} was purchased from Sigma-Aldrich. 1-Ethyl-3-methylimidazolium bis(trifluoromethylsulfonyl)amide, [EMIM][TFSI], was purchased from C-TRI Inc. The ion gel solution (10 wt% sample) was prepared by codissolving 100 mg of [EMIM][TFSI] and 1 g of P(VDF-HFP) in co-solvent of 4 ml of acetone and 2 ml of dimethylformamide. The solution was stirred at RT for 1 hr.

Fabrication of the ion gel nanofibers: Conventional electrospinning setup was used to spin the ion gel nanofibers. The prepared ion gel solution was loaded into a syringe and the distance between the needle and the collector is 15 cm. The process is conducted at 10 kV with the 1 ml/hr of feed rate. The nanofibers were collected on aluminum foil for 40 min at room temperature. The area of nanofibers was 16 cm × 16 cm and thickness was about 150 μm. The obtained samples were dried at 60 ^{o}C for 1 hr in air ambient. To fabricate the TENG, the spacer made of an insulating polymer film with double-side adhesives with a thickness of 0.03 mm was employed at the effective area (1 cm × 1 cm).

3.2 Photostimulated triboelectric generation

Preparation of Active blend layer: A mixture of Poly(3-hexylthiophene) (P3HT) (EMindex Co.) and [6,6]-phenyl C61-butyric acid methyl ester (PC61BM) (EMindex Co.) was used as the active layer. P3HT and $PC_{61}BM$(1:0.8) were dissolved in Dichlorobenzene at a concentration of 1wt. % and the P3HT:$PC_{61}BM$ solution, stirred overnight at 80 °C.

Preparation of TiO_x: Titanium(IV) isopropoxide (Ti[OCH(CH3)2]4, 99.999%,

Aldrich) was dissolved in isopropyl alcohol (IPA) at concentration of 0.2 vol.% and the Titanium isopropoxide solution was heated to 80 ℃ for 2h under magnetic stirring. The thickness of TiOx layer was controlled by concentration of Titanium isopropoxide solution (from 0.1 to 0.4 vol.%).

Device fabrication of P3HT/PCBM photovoltaics cell: All devices were fabricated on indium tin oxide (ITO) patterned glass substrates, which were cleaned by detergent and sonicated in deionized water, acetone, and isopropyl alcohol for 10 min, respectively. The ITO substrates were exposed to O_2 plasma for 20 min prior to spin-coating with poly(3,4-ethylenedioxythiophene):poly(styrenesulfonate) (PEDOT:PSS, AI 4083, Clevios) at 5000 rpm for 40 s. Next, the PEDOT:PSS-coated substrates were annealed at 140 °C for 10 min in air, and then taken into a nitrogen-filled glove box. The active blend layer of P3HT:$PC_{61}BM$ (EMindex Co.) was spin-coated onto PEDOT:PSS layer at 1100 rpm for 58 s. The Titanium isopropoxide solution was spin-coated onto the active blend layer at 4000 rpm for 40 s and was annealed at 80 ℃ 10min in air. Subsequently, thermal annealing was carried out in a glove box at 150 ℃ for 10 min. And then, Al (100nm) was thermally evaporated on to the TiO_x layer under vacuum condition (<10^{-6} Torr). The area of the Al electrode defines the active area of the device as 13.0 mm^2.

3.3 Measurement of characteristics

The scanning electron microscopy (SEM) was done using a PHILIPS XL30S with an accelerating voltage of 5 kV. The high-resolution transmission electron microscopy (HRTEM) images were collected using a Cs-corrected JEM-2100 operated at 200 kV. For cross-sectional TEM imaging, samples were milled with 30-kV-accelerated gallium ions using a focused ion beam machine (FIB; Quanta 3D FEG) in dual-beam mode.

The morphologies of ion gel nanofibers were characterized by field emission scanning electron microscope (FE-SEM). The thickness of ion gel nanofibers was measured using Hyrox optical analyzer. The microstructure and bonding status of ion gel were analyzed using XRD (PANalytical Inc., model no. X'pert-pro) and FTIR (Thermo Scientific Inc., model no. Nicolet iS 10). A pushing tester (Labworks Inc., model no. ET-126-4) was used to create a vertical compressive strain in the TENG. A Tektronix DPO 3052 Digital Phosphor Oscilloscope and a low-noise current preamplifier (model no. SR570, Stanford Research System, Inc.) were used for electrical measurements.

Power conversion efficiency was determined from *J–V* curve measurements (Iviumstat, Ivium Technologies, Eindhoven, The Netherlands) under a 1 sun, AM 1.5G spectrum from a solar simulator (Portable Solar Simulator PEC-L01, Peccell Technologies Inc., Kanagawa, Japan; 1000 Wm^{-2}).

AFM/KPFM Observation. To measure the surface potential of the device, Kelvin probe force microscopy (KPFM, Park Systems XE-70) measurements were performed with frequency modulation (FM) mode, using an Au/W-coated silicon tips (radius < 25nm, force constant 3 N m^{-1}, and resonance frequency of 75 kHz). 1 μm × 1 μm size KPFM images were scanned at a scanning speed of 0.5 Hz, and set at a point of 10 nm from a sample in atmospheric pressure at room temperature.

CHAPTER 4. ELECTROSTIMULATED TRIBOELECTRIC GENERATION

4.1 Introduction

Ionic liquid consisting of low molar mass cations and anions has attracted great attention in charge transport and electrochemical experiments.[1-3] To enhance the processability of employing ionic liquid in practical devices, it is desirable to blend ionic liquid with network-forming block copolymers. The results are referred to ion gels. Ion gels have demonstrated exceptional physical properties, such as high ionic conductivity, short polarization time, good thermal stability, and outstanding mechanical strength.[4-5] These advantages make ion gel a promising material for electrolyte of batteries, supercapacitor, organic/inorganic transistors, and electrochromic display.[6-8] Recently, the functionality of ion gels has expanded to flexible electrochemiluminescent.[9] Importantly, in most case, the ion gels are processed by spin coating or direct write printing, thus they have only bulk or 2D thin film structures.[10-11] However, comparing with nano-wire/dots structures, these kinds of structures have relatively small surface area and limited functionality. Thus, although the attention focused on ion gels has been increased in various research fields, its application has been limited to electrolyte materials in battery/capacitor and gate insulating materials in transistors. To our knowledge, there is no report on the formation of electrospun ion gels having nanofiber structure and their application for active materials in energy harvesting devices.

Among the various kinds of nanogenerators, the triboelectric nanogenerator (TENG), based on coupling with electrostatic effect have attracted much attention due to their high energy efficiency, simplicity, and scalability.[12-14] Thus, they have been applied to power source for electroplating, UV-detection, health care device, and chemical sensor.[15-18] Physical properties of triboelectric materials such as surface roughness, electron affinity, frictions and capacitance affect the performance of TENG and high capacitance is required to improve the output

performance (output voltage and current) of devices.[19-20] It is previously reported that the ion gel can form very high capacitance (~10 μF/cm^2) electrical double layer by externally applied bias.[21-22] Additionally, the capacitance of ion gel is independent of its thickness implying that we can control the thickness of triboelectric material in TENG from nano to micrometer scale.[5, 23] Thus, ion gel can be applied as a triboelectric material in TENG and improve the energy conversion efficiency.

4.2 Experimental details

Preparation of the ion gel solution; poly(vinylidene fluoride-*co*-hexafluoropropylene), P(VDF-HFP) with M_n = 130 000 g mol^{-1} and M_w = 400 000 g mol^{-1} was purchased from Sigma-Aldrich. 1-Ethyl-3-methylimidazolium bis(trifluoromethylsulfonyl)amide, [EMIM][TFSI], was purchased from C-TRI Inc. The ion gel solution (10 wt% sample) was prepared by codissolving 100 mg of [EMIM][TFSI] and 1 g of P(VDF-HFP) in co-solvent of 4 ml of acetone and 2 ml of dimethylformamide. The solution was stirred at RT for 1 hr.

Fabrication of the ion gel nanofibers: Conventional electrospinning setup was used to spin the ion gel nanofibers. The prepared ion gel solution was loaded into a syringe and the distance between the needle and the collector is 15 cm. The process is conducted at 10 kV with the 1 ml/hr of feed rate. The nanofibers were collected on aluminum foil for 40 min at room temperature. The area of nanofibers was 16 cm × 16 cm and thickness was about 150 μm. The obtained samples were dried at 60 ^{o}C for 1 hr in air ambient. To fabricate the TENG, the spacer made of an insulating polymer film with double-side adhesives with a thickness of 0.03 mm was employed at the effective area (1 cm × 1 cm).

Characterization and Measurement: The morphologies of ion gel nanofibers were characterized by field emission scanning electron microscope (FE-SEM). The thickness of ion

gel nanofibers was measured using Hyrox optical analyzer. The microstructure and bonding status of ion gel were analyzed using XRD (PANalytical Inc., model no. X'pert-pro) and FTIR (Thermo Scientific Inc., model no. Nicolet iS 10). A pushing tester (Labworks Inc., model no. ET-126-4) was used to create a vertical compressive strain in the TENG. A Tektronix DPO 3052 Digital Phosphor Oscilloscope and a low-noise current preamplifier (model no. SR570, Stanford Research System, Inc.) were used for electrical measurements.

4.3 Electrical double layers formed at the ion gel/electrode interfaces

In this study, we extend the functionality of ion gels to demonstrate electrical energy harvesting TENG. To enhance the power output performance, we employed nanofibers structured ion gels as a triboelectric material. Using conventional electrospinning technique, we can fabricate large area (16 cm × 16 cm) ion gel nanofibers mat having thickness ranges from 10 – 1000 μm. We designed TENG by using bare polymer (poly(vinylidene fluoride-*co*-hexafluoropropylene), P(VDF-HFP)) and ion gel nanofibers. Comparing with spin coated film based TENG (3 V and 5 μA/cm^2), the device having P(VDF-HFP) nanofibers structure which fabricated by electrospinning showed enhanced output power (20 V and 19 μA/cm^2). By doping ionic liquid 1-ethyl-3-methylimidazolium bis(trifluoromethylsufonyl)amide [EMIM][TFSI] into the P(VDF-HFP), we could fabricate ion gels nanofibers and the output open-circuit voltage and short-circuit current density from the TENG increases up to a high value of 45 V and 49 μA/cm^2, respectively, under same cycled compressive force. When compressive force applied into the TENG with ion gels, positive and negative charges generated by triboelectric effect attract counterions in the ion gels and large capacitance (> 10 μF/cm^2) electrical double layers formed at the ion gel/electrode interfaces, resulting in improved output power. We also evaluated the device stability and the ion gel nanofiber based TENGs exhibited good stability under continuous operation over 10,000 cycles. Overall, the results indicate that the nanofiber

structured ion gel provides a convenient route to incorporate an active layer in energy harvesting devices.

4.4 Results and Discussion

4.4.1 Ion gel nanofiber structured triboelectric nanogenerator

For TENG, large surface area and rough surfaces of triboelectric layer can generate more surface charge and triboelectric effect, result in high output power.[24-25] Thus, in this work we fabricated nanofibers structured ion gel by the electrospinning technique to enhance the triboelectric effect. Electrospinning technique is a simple and effective method capable of fabricating polymer nanofibers with diameters down to a few nanometers.[26-27] The electrospinning setup which consists of an ion gel solution container, a syringe pump, a grounded collector, and a high voltage power supply is shown in Figure 4a and 4b. Under a high DC voltage (electric field), the solution surface was highly charged and a number of ion gel jets were generated. These jets moved and deposited on the collector forming nanofiber structures. The aluminum foil was put on the collector plate as a receiver substrate. By controlling the collecting time, we can control the area and thickness of ion gel nanofibers. The collecting time to produce a 150 μm-thick ion gel nanofibers mat of a 16 cm × 16 cm was about 40 min (Figure 4c). Figure 4d schematically illustrates the structure of the TENG with ion gel nanofibers. To fabricate the TENG, we used Al foil as a bottom electrode. A spacer made by insulating polymer was staked on the ion gel nanofiber mat. A Kapton film which act as a triboelectric material coated Al electrode was used as a top electrode.

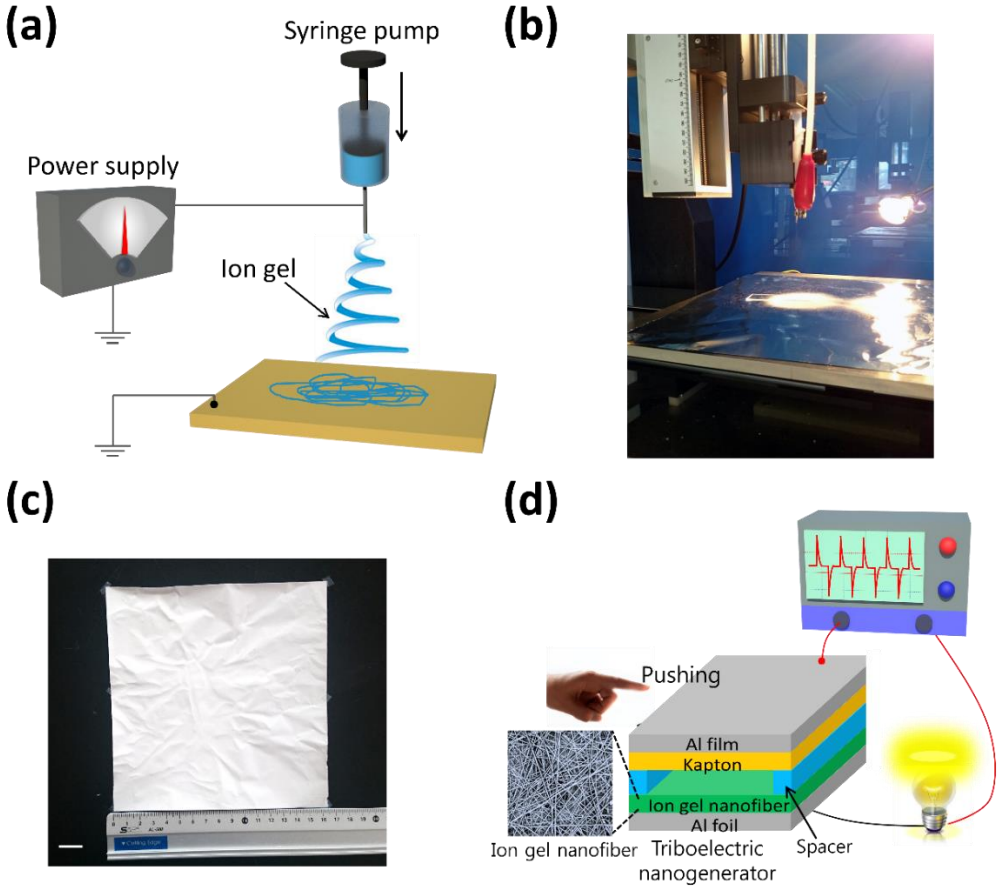

Figure 4. (a) Schematic diagram of the electrospinning set-up used in this work. (b) Digital photo of electrospinning process for fabrication of ion gel nanofibers. The fibers were collected on the surface of a collector covered with aluminum foil. (c) Photo of a large piece of 150 μm-thick ion gel nanofibers mat prepared by electrospinning (16 cm ×16 cm, scalebar: 1 cm). (d) Structure and illustration of triboelectric nanogenerator with ion gel nanofibers.

4.4.2 Ion gel nanofibers with different ionic liquid concentrations

Figure 5a-d show the scanning electron microscopy (SEM) images of electrospun ion gel nanofibers with different ionic liquid concentrations (0, 2, 5, and 10 wt%). For example, 10 wt% ion gel was prepared by adding 0.1 g of ionic liqud and 0.9 g of P(VDF-HFP) to sovent. Smooth and bead-free solid fibers in the form of randomly oriented fiber web were obtained for all the samples. As increased the ionic liquid concentration, the shape of nanofibers for each

sample did not show any noticeable changes. However, slight changes in the nanofibers diameters and distribution were found. The average diameter of 0 wt % sample (bare P(VDF-HFP)) was 482 ± 160 nm. For 10 wt% ion gel sample, the average diameter decreased to 457 ± 192 nm. This is due to the increment of the charge density in the solution containing anions and cations that cause stronger elongation force on the ejected jets under the same electric field. During the electrospinning process, the jet is stretched and bended due to the interaction between elastic forces and applied electronic field.[28-29] Because the ions in the ion gel induce high charge densities to the jet, bending instabilities occur at high concentration samples, resulting in reduced diameter and wide diameter distribution.

4.4.3 Crystalline structure of the ion gel nanofibers

To investigate the crystalline structure of the ion gel nanofibers, Fourier transform infrared (FTIR) and X-ray diffraction (XRD) analysis were performed on each sample. The vibrational bands at 1180, 986, and 741 cm^{-1} in bare (0 wt%) P(VDF-HFP) sample are attributed to the non-polar α-phase in Figure 5a.[30-31] The characteristic peaks at 1276 and 841 cm^{-1} correspond to the β-phase. We can also observe a weak shoulder peak related γ-phase at 1232 cm^{-1}. With addition of ionic liquid [EMIM][TFSI], several peaks in the region between 500 and 750 cm^{-1} were observed. These peaks are assigned to a CF_3 antisymmetric bending, a SO_2 antisymetmetric bending, a S-N-S bending, and a CF_3 symmetric bending in [TFSI] anion.[32]

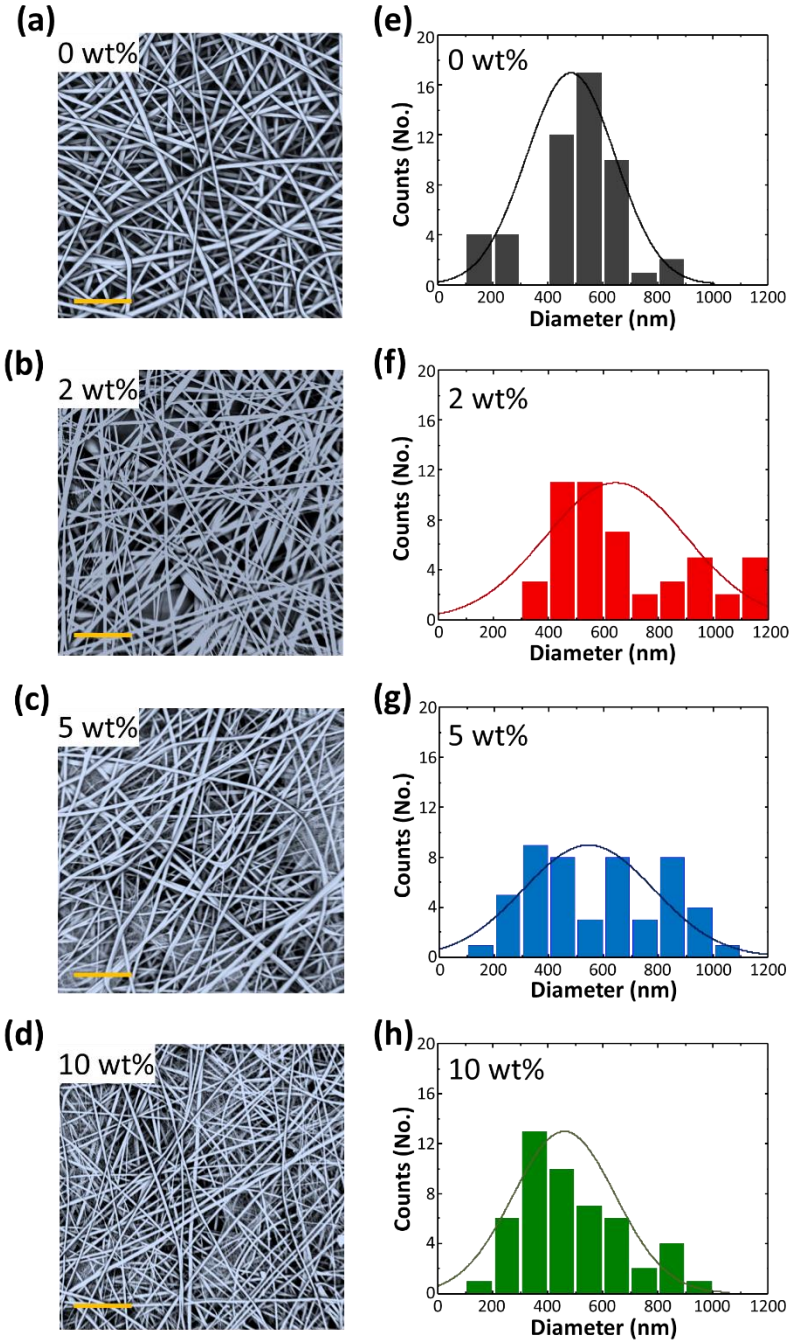

Figure 5. (a-d) SEM images of ion gel mats doped with different doping ratios of ionic liquid, [EMIM][TFSI] (0-10 wt%). Scalebar: 1 μm. (e-h) The bar charts showing the fiber diameter distribution of electrospun ion gel as a function of doping concentration. The average diameter of P(VDF-HFP) (0 wt%) and ion gel (10 wt%) sample were 482 nm and 457 nm, respectively.

Newly appeared peaks at 1132 and 1348 cm^{-1} imply SO_2 symmetric stretching and antisymmetric stretching, respectively. On the basis of these findings, it is suggested that the electrospun P(VDF-HFP) and ion gel nanofibers have a mixed-crystal structure comprising α-phase, β-phase, and very small amount of γ-phase. The existence of α-phase and β-phase in nanofibers confirmed by XRD data which had a strong β-phase crystalline signal with 2θ at 20.5^{o} which is assigned to the total diffraction in (110) and (200) plane in Figure 5b).[30-31] Due to elongation forces and stretching during electrospinning process, formation of the polar β-phase was promoted. The peak at 18.6^{o} corresponds to the reflection of the (020) plane of the α-phase. As increased the ionic liquid concentration, the shape and peak position of XRD data for each sample did not show any noticeable changes, indicating that the presence of cations and anions has a negligible effect on crystal structure of nanofibers.

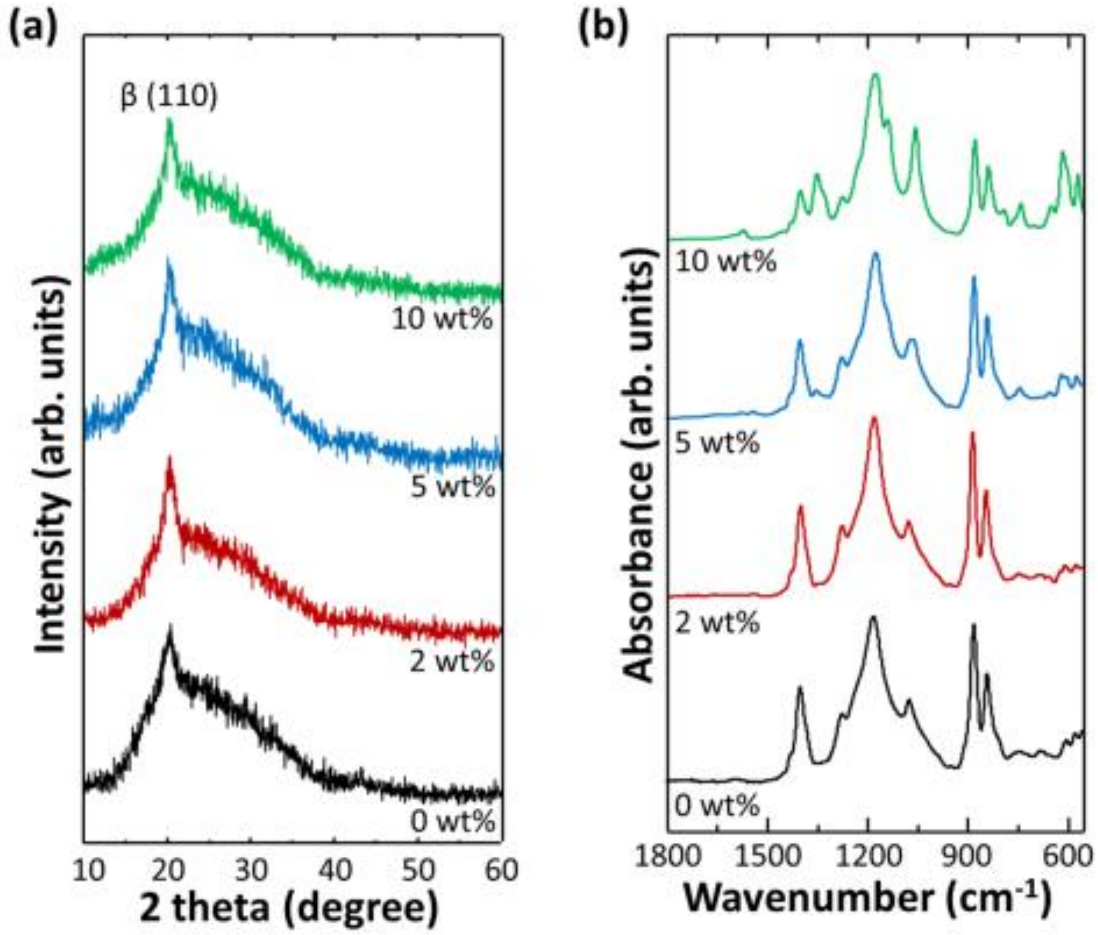

Figure 6. (a) XRD patterns of the ion gel nanofibers as a function of doping concentrations. The characteristic peak with 2θ at 20.5 ° is assigned to the total diffraction in the (110) and (200) planes. The peak at 18.6 ° corresponds to the reflection of the (020) plane of the α-phase. (b) The FTIR spectra of ion gel nanofibers with different ionic liquid doping concentrations. Vibrational bands at 1276, 841, and 1232 cm^{-1} are attributed to the β-phase and γ-phase of P(VDF-HFP). Newly appeared peaks at 1152, 796, and 613 cm^{-1} are related to the α-phase of P(VDF-HFP). Several peaks in the region between 1348, 1132, 500 and 750 cm^{-1} are assigned to [EMIM][TFSI] related peaks.

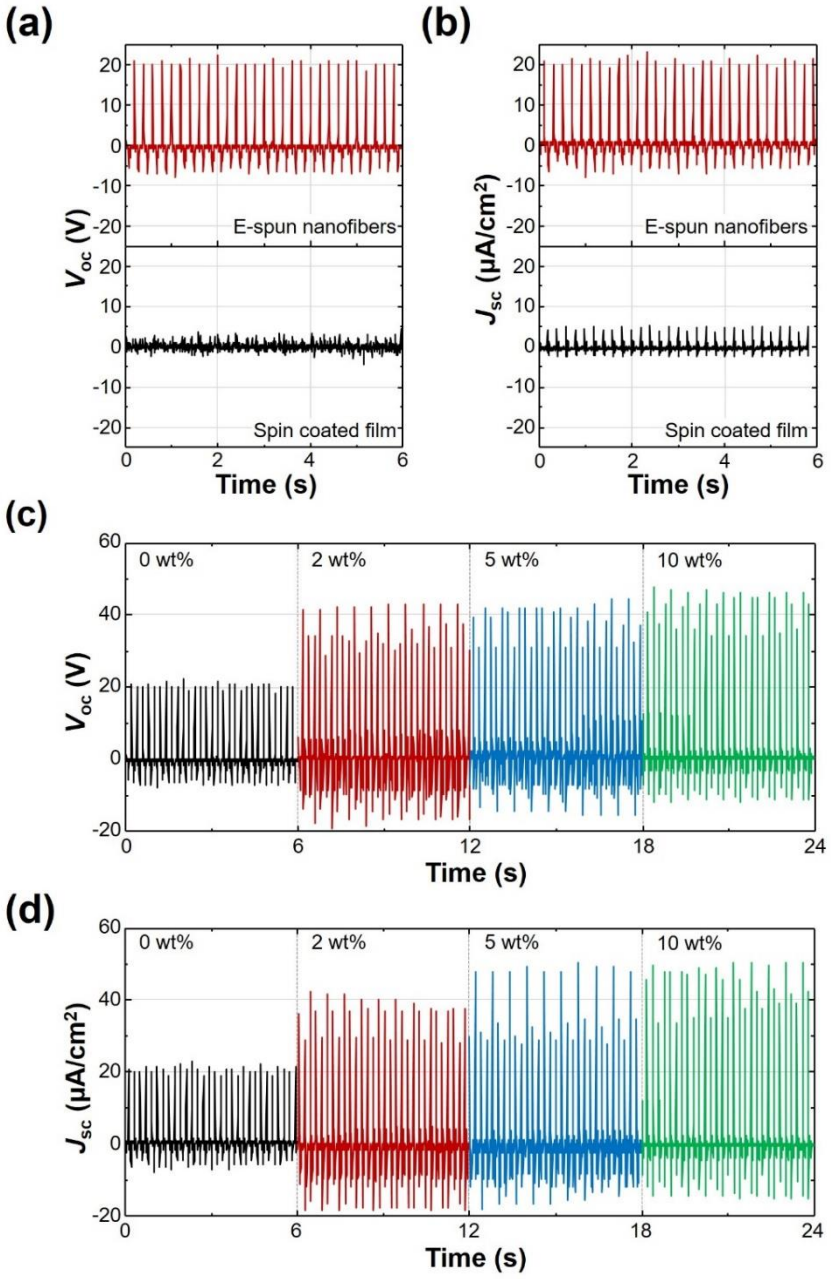

Figure 7. (a) Output open-circuit voltage and (b) short-circuit current density of the TENG composed of spin coated P(VDF-HFP) film and electrospun nanofibers. The active area of device was 1 cm × 1 cm. (c-d) Electrical output performance of the ion gel nanofibers based TENG with various ionic liqid doping concentrations (0-10 wt%) under same mechanical force (90 N).

4.4.4 Output performance

Figure 7a and 7b show the output open-circuit voltage and short-circuit current density, generated by the P(VDF-HFP) nanofibers based TENG, under a cycled compressive force of 90 N at an applied frequency of 5 Hz. To compare the output performance of nanofibers-structured mat over flat films, a nanogenerator having spin coated P(VDF-HFP) triboelectric materials (flat surface) was also fabricated and evaluated. Both devices generated typical AC-type signal. The output open-circuit voltages of TENGs with P(VDF-HFP) nanofibers structure and flat surface are 20 V and 3 V, respectively under same mechanical force. There are 6.2 times increase in short-circuit current density. One of the advantages of electrospinning is that it can fabricate various kinds of polymer nanofibers.[29]

Thus, we also fabricated TENGs using electospun polyvinyl pyrrolidone (PVP), polystyrene (PS), and polymethyl methacrylate (PMMA) nanofibers and they also exhibited typical TENG output performance in Figure 8. This result implies that the nanofibers prepared by the electrospinning method are effective in improving the output performance of TENG. To confirm that the measured output performance was originated from the TENG and eliminate the influence of the noise caused by the measuring system, we changed the way of the connection of the device (switching polarity) with the measurement equipment in Figure 9.

The connecting configuration that the positive probe connecting with the P(VDF-HFP) nanofibers and the negative probe connecting with the Kapton film is defined as the forward connection and the inverted connecting is defined as the reverse connection. As we reversed the connection of the open-circuit voltage and short-circuit current meters, the output signals were reversed, as shown in Figure 9, implying the output signals are generated by triboelectric effect.

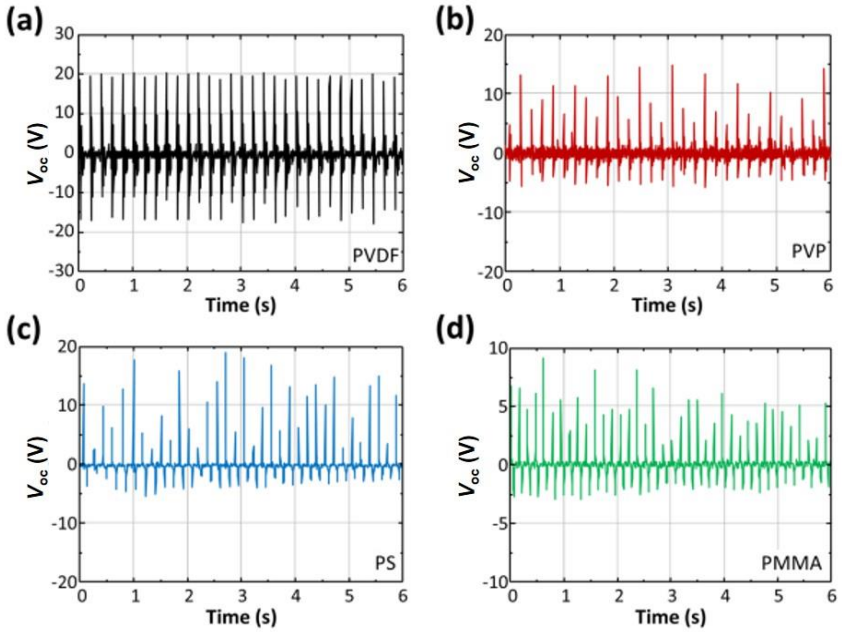

Figure 8. Output open-circuit voltage characteristics of TENGs with various polymer nanofibers as triboelectric materials. All polymer nanofibers were fabricated using an electrospinning process. (a) PVDF, (b) PVP, (c) PS, (d) PMMA.

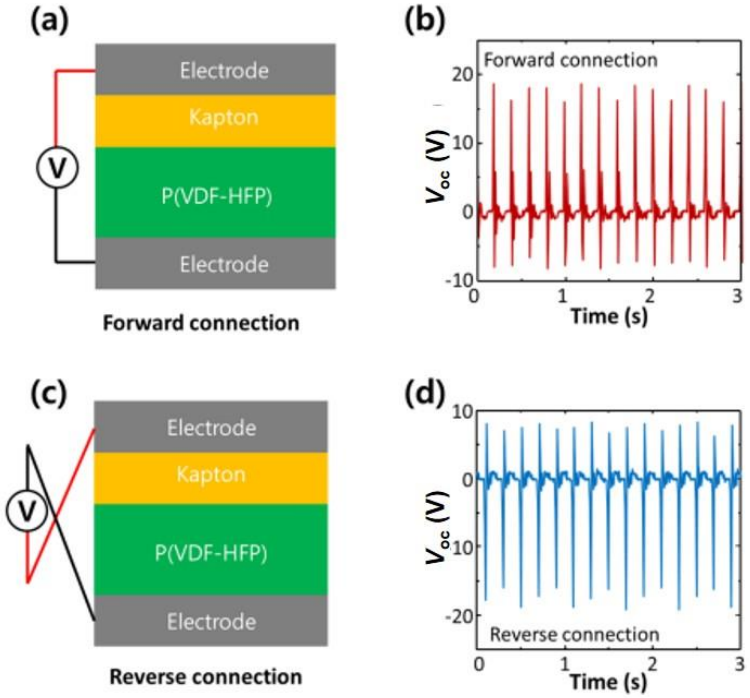

Figure 9. Output open-circuit voltage signal of TENG under the (a-b) forward and (c-d) reverse connections.

4.4.5 Mechanism of charge transfer

When we employed electrospun ion gel nanofibers instead of bare P(VDF-HFP), the device showed improved output performance (Figure 7c and 7d). For 2 wt%-device, the output open-circuit voltage and short-circuit current density reached 42 V and 38 μA/cm^2, respectively. The values were increased to 45 V and 49 μA/cm^2 for 10 wt%-device. The enhancement in the electrical power generation by the doping of ionic liquid can be explained by the increased inductive charges in the triboelectric layer. Initially, no charge is inducted with no electric potential difference between two electrodes of P(VDF-HFP) based TENGs (Figure 10a). With an externally applied compressive force, the P(VDF-HFP) and Kapton brought into contact with each other. Then, surface charge transfer takes place at the interfaces due to the triboelectric effect.

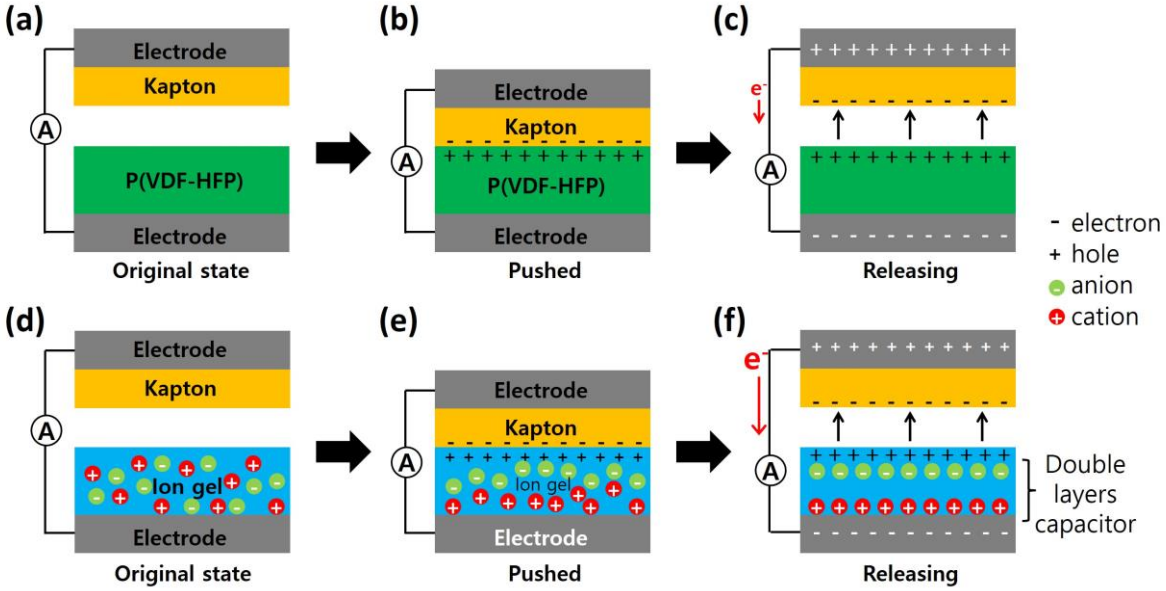

Figure 10. Schematic diagram of electric power generation process of (a-c) bare P(VDF-HFP) and (d-f) ion gel based triboelectric nanogenerators.

According to the tribielectric series, Kapon film has strong negative triboelectric polarity.[19] Thus, negative and positive charges are induced at the Kapton and P(VDF-HFP) surfaces, respectively. Because of insulating property of the P(VDF-HFP) and Kapton, the transferred charges are confined at the each surface and leading no electric potential difference between two electrode (Figure 10b). When the pressure is released, the P(VDF-HFP) and Kapton surfaces are separated from each other. In this stage, the dipole moment becomes stronger and a strong electric potential difference is generated between the electrodes. Thus, electrons start to flow from the negative potential to the positive potential and charges are accumulated on the electrodes, resulting in a positive electrical signal (Figure 10c). When compressive force is applied to ion gel based TENG, the confined charges attract counterions. At the releasing stage, positive and negative ions accumulate at the Kapton/ion gel and ion gel/electrode interfaces, forming a 2D electrical double layer (EDL) (Figure 7d-f). It is previously reported that the ideal capacitance of the EDL is very large value about > 10 F/cm^2.[22] We calculated the triboelectric charge density (σ) using the equation ($\sigma = V\varepsilon_0/d$, ε_0 and d are vacuum permittivity and spacer height, respectively) and lager σ value (13.3 C/m^2) of ion gel based TENG than that of P(VDF-HFP) based one (5.2 C/m^2) might be originated from the formation of EDL. A current (I) generated across the TENG is a function of potential across the two electrodes and change in the capacitance (C) of the system,[19]

$$I = C\frac{\partial V}{\partial t} + V\frac{\partial C}{\partial t}$$

Thus, mobile ions in the ion gel induced formation of EDLs and large capacitance value, resulting in improved output performance of nanogenerator. For 20 wt%-TENG, the device showed much reduced output open-circuit voltage and short-circuit current in Figure 11. This result can be explained by the triboelectric material-to-electrolyte transition in ion gel nanofibers. Output power data in Figure 7 suggests that the ion gel nanofibers behaves as a

triboelectric materials for ionic liquid concentrations up to 10 wt%. Above this concentration, the output power of generator drastically degraded indicating that ion gel nanofibers act as an electrolyte. This finding will need considerably more investigation for clear understand.

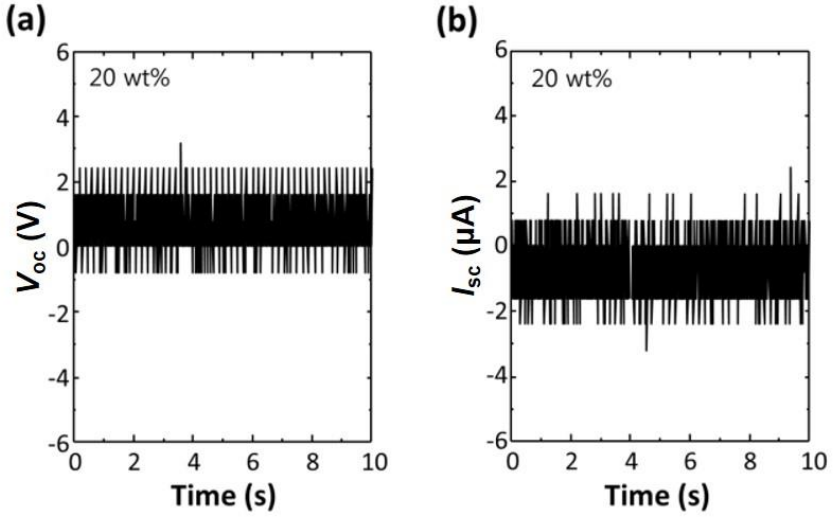

Figure 11. (a) Output open-circuit voltage and (b) short-circuit current characteristics of TENG with 20 wt% ion gel nanofibers.

4.4.6 Stability of ion gel based TENG

We have performed durability/stability test of ion gel based TENG (10 wt%) to confirm the mechanical stability of the device. Figure 12a and 12b show the open-circuit voltage and short-circuit current of a TENG that was operated continuously at 5 Hz for 10,000 cycles. After the test, the device still displayed clear power generating performance. As plotted in Figure 12c, only a slight decline (~5%) was observed for the output open-circuit voltage after a total of 10,000 working cycles.

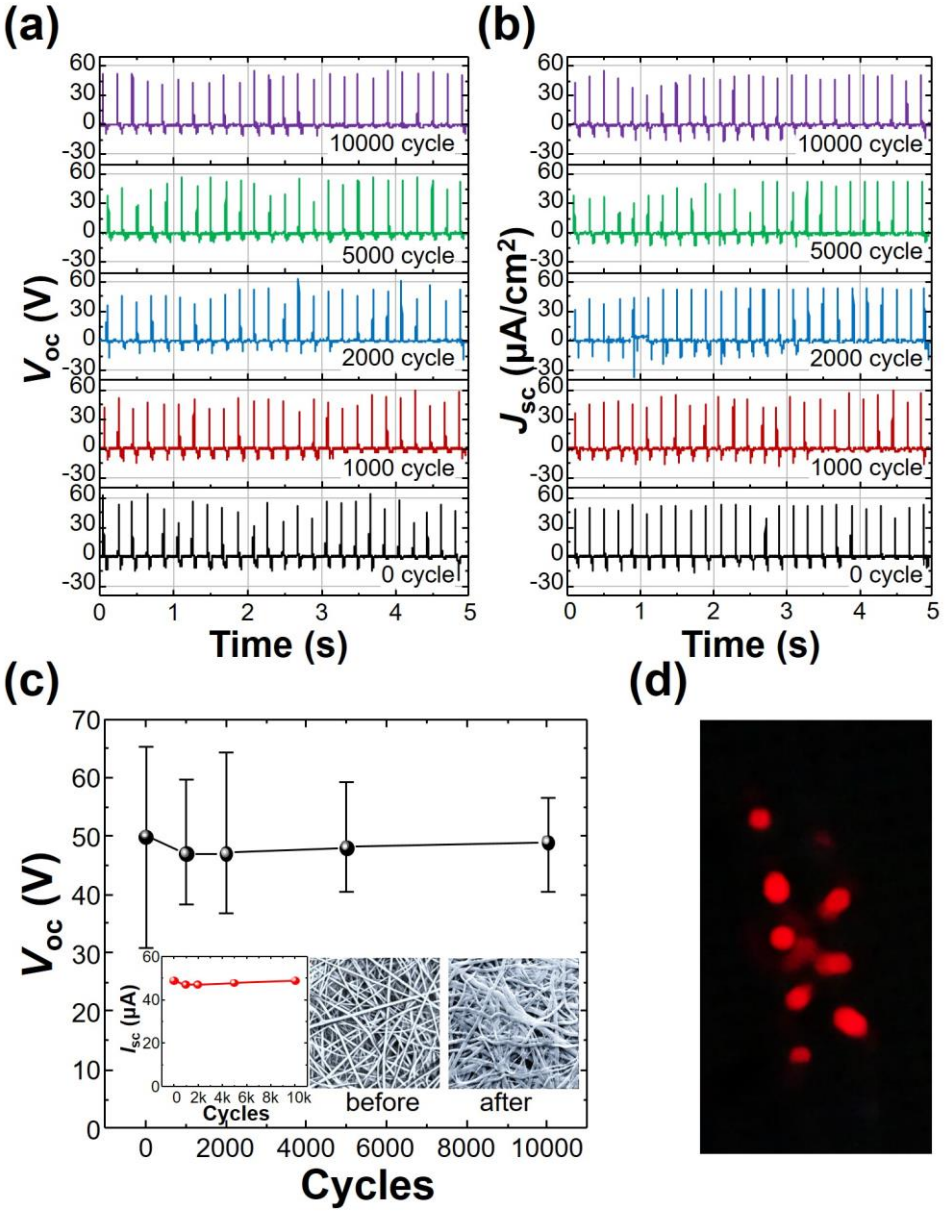

Figure 12. Operational stability of ion gel based TENG. (a) open-circuit voltage and (b) short-circuit current density characteristics of a TENG operated continuously for 10,000 cycles, acquired at f = 5 Hz. (c) Change of output open-circuit voltage of a TENG as a function of operating cycle. Inset: Change of short-circuit current for a TENG and SEM images (100 μm × 100 μm) of ion gel nanofibers (10 wt%) surface before and after 10,000 cyclic operation. (d) A snapshot of the 15-LEDs arrays lit up by the power output generated from the TENG.

This slight degradation of TENG might originate from the deformed surface morphology of ion gel nanofibers. Before the test, the ion gel exhibited clear nanofibers structure. After the test, however, the nanofibers are deformed by the cyclic compressive stress (Inset in Figure 12c). It is noteworthy that although the surface of ion gel nanofibers was deformed by the continuous cyclic stress, the output performance of TENG could be maintained. To study a practical application of the TENG, we drove series-connected light emitting diodes (LEDs) using solely the output power from an ion gel based TENG. Red LEDs was directly connected to the output of the TENG without any capacitor and rectifier. Figure 12d presents the images of the photo taken after the TENG was activated. The output power from the TENG (10 wt%) was able to light up more than 15-LEDs instantaneously and simultaneously. P(VDF-HFP) based TENG, however, lit up 10 LEDs under the same compressive force (not shown in here). From these results, we confirmed that ion gel nanofibers can be suitable for high performance TENG.

4.5 Conclusion

In conclustion, we have successfully demonstrated the application of electrospun ion gel nanofibers as a triboelectric materials of TENG. The novelty of this work lies in (1) the fabrication of large area ion gel nanofibers using simple electrospinning method and (2) the first demonstration of an energy harvesting application of ion gel nanofibers using the triboelectric effect. Using electrospinning method, we fabricated large area (16 cm × 16 cm) ion gel nanofibers mat and the nanofibers have average diameter of 457 nm. A large output open-circuit voltage and short-circuit current densityof up to 45 V and 49 $\mu A/cm^2$, respectively could be obtained from the ion gel based TENG in comparison to the electrical output obtained from the bare polymer P(VDF-HFP) based one (20 V and 19 $\mu A/cm^2$, respectively), under the same mechanical force. The improvement in the electrical power output of ion gel based TENG

was explained in term of the formation of electrical double layer in triboelectric materials. In addition, the TENG exhibited good stability under continuous operation. We also could power 15-LEDs using the electrical power output of the TENG without other external energy source and rectifier. Based on the excellent output performance and stability, this simple but effective nanofiber-structured ion gel opens up the new opportunity for the application to the powering portable devices and self-powered electronic system. Future work will focus on achieving fabric based energy devices and on developing practical power source for electronic applications.

4.6 Reference

[1] J. Le Bideau, L. Viau, and A. Vioux, *Chem. Soc. Rev.* **2011**, *40*, 907.

[2] Y. Lu, K. Korf, Y. Kambe, Z. Tu, and L. A. Archer, *Angew. Chem. Int.* **2014**, *53*, 488.

[3] R. D. Rogers, and K. R. Seddon, *Science* **2003**, *302*, 792.

[4] Y. Gu, S. Zhang, L. Martinetti, K. H. Lee, L. D. McIntosh, C. D. Frisbie, and T. P. Lodge, *J. Am. Chem. Soc.* **2013**, *135*, 9652.

[5] K. H. Lee, S. Zhang, T. P. Lodge, and C. D. Frisbie, *J. Phys. Chem. B* **2011**, *115*, 3315.

[6] M. Deepa, A. Awadhia, and S. Bhandari, *Phys. Chem. Chem. Phys.* **2009**, *11*, 5674.

[7] K. H. Lee, M. S. Kang, S. Zhang, Y. Gu, T. P. Lodge, and C. D. Frisbie, *Adv. Mater.* **2012**, *24*, 4457.

[8] X. Liu, D. Wu, H. Wang, and Q. Wang, *Adv. Mater.* **2014**, *26*, 4370.

[9] H. C. Moon, T. P. Lodge, and C. D. Frisbie, *J. Am. Chem. Soc.* **2014**, *136*, 3705.

[10] J. H. Cho, J. Lee, Y. Xia, B. Kim, Y. He, M. J. Renn, T. P. Lodge, and C. D. Frisbie, *Nat. Mater.* **2008**, *7*, 900.

[11] B. J. Kim, H. Jang, S. K. Lee, B. H. Hong, J. H. Ahn, and J. H. Cho, *Nano Lett.* **2010**, *10*, 3464.

[12] Y. H. Ko, G. Nagaraju, S. H. Lee, and J. S. Yu, *ACS Appl. Mater. Interfaces* **2014**, *6*, 6631.

[13] K. Y. Lee, J. Chun, J. H. Lee, K. N. Kim, N. R. Kang, J. Y. Kim, M. H. Kim, K. S. Shin, M. K. Gupta, J. M. Baik, and S. W. Kim, *Adv. Mater.* **2014**, *26*, 5037.

[14] Y. Yang, H. Zhang, and Z. L. Wang, *Adv. Func. Mater.* **2014**, *24*, 3745.

[15] Y. Yang, L. Long, Z. Yue, J. Qingshen, H. Te-Chien, and W. Zhong Lin, *ACS Nano* **2012**, *6*, 10378.

[16] S. Kim, M. K. Gupta, K. Y. Lee, A. Sohn, T. Y. Kim, K. S. Shin, D. Kim, S. K. Kim, K. H. Lee, H. J. Shin, D. W. Kim, and S. W. Kim, *Adv. Mater.* **2014**, *26*, 3918.

[17] X. S. Zhang, M. D. Han, R. X. Wang, F. Y. Zhu, Z. H. Li, W. Wang, and H. X. Zhang, *Nano Lett.* **2013**, *13*, 1168.

[18] G. Zhu, C. Pan, W. Guo, C. Y. Chen, Y. Zhou, R. Yu, and Z. L. Wang, *Nano Lett.* **2012**, *12*, 4960.

[19] F.-R. Fan, Z.-Q. Tian, and Z. Lin Wang, *Nano Energy* **2012**, *1*, 328.

[20] F. R. Fan, L. Lin, G. Zhu, W. Wu, R. Zhang, and Z. L. Wang, *Nano Lett.* **2012**, *12*, 3109.

[21] S. H. Kim, K. Hong, K. H. Lee, and C. D. Frisbie, *ACS Appl. Mater. Interfaces* **2013**, *5*, 6580.

[22] S. H. Kim, K. Hong, W. Xie, K. H. Lee, S. Zhang, T. P. Lodge, and C. D. Frisbie, *Adv. Mater.* **2013**, *25*, 1822.

[23] K. Hong, S. H. Kim, K. H. Lee, and C. D. Frisbie, *Adv. Mater.* **2013**, *25*, 3413.

[24] Y. Yang, Y. S. Zhou, H. Zhang, Y. Liu, S. Lee, and Z. L. Wang, *Adv. Mater.* **2013**, *25*, 6594.

[25] S. Wang, L. Lin, and Z. L. Wang, *Nano Lett.* **2012**, *12*, 6339.

[26] Y. Liu, X. Zhang, Y. Xia, and H. Yang, *Adv. Mater.* **2010**, *22*, 2454.

[27] J. H. Park, and P. V. Braun, *Adv. Mater.* **2010**, *22*, 496.

[28] D. Li, and Y. Xia, *Adv. Mater.* **2004**, *16*, 1151.

[29] A. Greiner, and J. H. Wendorff, *Angew. Chem. Int.* **2007**, *46*, 5670.

[30] J. Fang, X. Wang, and T. Lin, *J. Mater. Chem.* **2011**, *21*, 11088.

[31] H. Yu, T. Huang, M. Lu, M. Mao, Q. Zhang, and H. Wang, *Nanotechnology* **2013**, *24*, 405401.

[32] J. Kiefer, J. Fries, and A. Leipertz, *Appl Spectroscopy* **2007**, *61*, 1306.

CHAPTER 5. PHOTOSTIMULATED TRIBOELECTRIC GENERATION

5.1 Introduction

Contact electrification is a well-known phenomenon occurring when two objects get in touch each other, i.e. the objects become spontaneously and oppositely charged due to the charge transfer between them, which intrinsically depends on the intrinsic properties of the objects according to the triboelectric series. The contact electrification phenomenon has allowed the construction of frictional electrostatic generators such as Van de Graaff generator, Lorentz generator, and Holtz machine, but it was also fully utilized in many applications such as chemical sensors, electrostatic charge patterning, and laser printing[1-5]. Recently, triboelectric nanogenerator (TENG) coupled with electrostatic effect was proposed as new energy generating device. Many possible applications such as environmental/infrastructure monitoring, wearable devices, implantable devices, charging portable electronics and self-powered sensors (i.e. pressure, motion, acoustic sensor) are successfully demonstrated so far.[6-12] Although there are still many issues to be solved, some technologies are good enough to reach commercialization.

Although the charge transfer has been studied so long, the rapid development of new nanomaterials and the wide potential applications of the triboelectrification-based technologies increased the needs to enhance the fundamental understanding of the phenomena due to the complex interaction between many factors affecting the charge transfer. In general, the generated potential between two objects was known to be determined by the density of charges transferred.[13] The charge density significantly depends on the physical and chemical properties of the materials as well as many environmental factors (i.e. relative humidity, temperature, and pressure). The probability of the charge transfer is determined by the band alignment of two different materials, thus, control over the work function is the key to

increasing the charge density.[14-15] Various surface modifications technologies such as plasma treatments, self-assembled monolayers, aligned dipole moment etc., were applied to control the surface potential and were proven to be so effective. Light-induced surface potential change was also reported to be quite useful in fabricating photodetectors based on the triboelectrification. However, most of the works have focused on the triboelectric negative materials except of extremely few papers. Furthermore, there was no report on the increase of the surface charge density by the light illumination.

Here, we report the light-induced unusual inversion in charge transfer and increase of the tribo-charges during the physical contact at the oxide/polyimide interface. In particular, the wavelength-dependent response of the TENG's output performance is demonstrated. The amorphous titanium oxide (TiO_x), playing as a triboelectric positive layer donating electrons, was deposited on the P3HT:PC_{61}BM/PEDOT:PSS on ITO/glass substrate. The polyimide layer, followed by the deposition of aluminum (Al), was placed on the TiO_x, by having the two physically separated. When the polyimide and TiO_x are touched and released together, the generated potential produced between them makes the electrons flow through the outer circuit connected between them. Here, we found that the direction of electron flow was reversed after the light was illuminated onto the interface, meaning the inversion of charge transfer, not reported yet. By Kelvin probe force microscope (KPFM) measurement of the TiO_x layer and the wavelength-dependent study of the TENGs, it was concluded that the photogenerated electrons from active layer are accumulated at the surface of TiO_x, decreasing the effective work function. It was clearly supported by measuring the output open-circuit voltages of gate-voltage controlled TENG. We also compared them with TiO_x on ITO/glass and TiO_2 on ITO/glass as refences.

5.2 Experimental details

Preparation of Active blend layer: A mixture of Poly(3-hexylthiophene) (P3HT) (EMindex Co.) and [6,6]-phenyl C61-butyric acid methyl ester (PC61BM) (EMindex Co.) was used as the active layer. P3HT and $PC_{61}BM$(1:0.8) were dissolved in Dichlorobenzene at a concentration of 1wt. % and the P3HT:$PC_{61}BM$ solution, stirred overnight at 80 ℃.

Preparation of TiO_x: Titanium(IV) isopropoxide (Ti[OCH(CH3)2]4, 99.999%, Aldrich) was dissolved in isopropyl alcohol (IPA) at concentration of 0.2 vol.% and the Titanium isopropoxide solution was heated to 80 ℃ for 2h under magnetic stirring. The thickness of TiOx layer was controlled by concentration of Titanium isopropoxide solution (from 0.1 to 0.4 vol.%).

All devices were fabricated on indium tin oxide (ITO) patterned glass substrates, which were cleaned by detergent and sonicated in deionized water, acetone, and isopropyl alcohol for 10 min, respectively. The ITO substrates were exposed to O_2 plasma for 20 min prior to spin-coating with poly(3,4-ethylenedioxythiophene):poly(styrenesulfonate) (PEDOT:PSS, AI 4083, Clevios) at 5000 rpm for 40 s. Next, the PEDOT:PSS-coated substrates were annealed at 140 ℃ for 10 min in air, and then taken into a nitrogen-filled glove box. The active blend layer of P3HT:$PC_{61}BM$ (EMindex Co.) was spin-coated onto PEDOT:PSS layer at 1100 rpm for 58 s. The Titanium isopropoxide solution was spin-coated onto the active blend layer at 4000 rpm for 40 s and was annealed at 80 ℃ 10min in air. Subsequently, thermal annealing was carried out in a glove box at 150 ℃ for 10 min. And then, Al (100nm) was thermally evaporated on to the TiO_x layer under vacuum condition (<10^{-6} Torr). The area of the Al electrode defines the active area of the device as 13.0 mm^2.

Power conversion efficiency was determined from *J–V* curve measurements (Iviumstat,

Ivium Technologies, Eindhoven, The Netherlands) under a 1 sun, AM 1.5G spectrum from a solar simulator (Portable Solar Simulator PEC-L01, Peccell Technologies Inc., Kanagawa, Japan; 1000 Wm^{-2}).

A pushing tester (Labworks Inc., model no. ET-126–4) was used to create a vertical compressive strain in the nanogenerator. A Tektronix DPO 3052 Digital Phosphor Oscilloscope and a low-noise current preamplifier (model no. SR570, Stanford Research Systems, Inc.) were used for electrical measurements. AFM/KPFM Observation. To measure the surface potential of the device, Kelvin probe force microscopy (KPFM, Park Systems XE-70) measurements were performed with frequency modulation (FM) mode, using an Au/W-coated silicon tips (radius < 25nm, force constant 3 N m^{-1}, and resonance frequency of 75 kHz). 1 μm × 1 μm size KPFM images were scanned at a scanning speed of 0.5 Hz, and set at a point of 10 nm from a sample in atmospheric pressure at room temperature.

5.3 Results and Discussion

5.3.1 Photovoltaic structured triboelectric nanogenerator

A schematic diagram of the TENGs structure is shown in Figure 13a. The TENG consists of Al/Polyimide/TiO_x/P3HT:PC_{61}BM/PEDOT:PSS/ITO/glass (Fig. 13b), by having the two (polyimide and TiO_x) physically separated, as described in the Experimental section. Before the output power measurement, an organic photovoltaic structure with Al/TiO_x/P3HT:PC_{61}BM/PEDOT:PSS/ITO/glass was fabricated in Figure 14a and the current-density versus voltage *(J–V)* characteristics were evaluated under AM1.5G illumination from a calibrated solar simulator with an irradiation intensity of 100 mW/cm^2, plotted in Figure 14b.

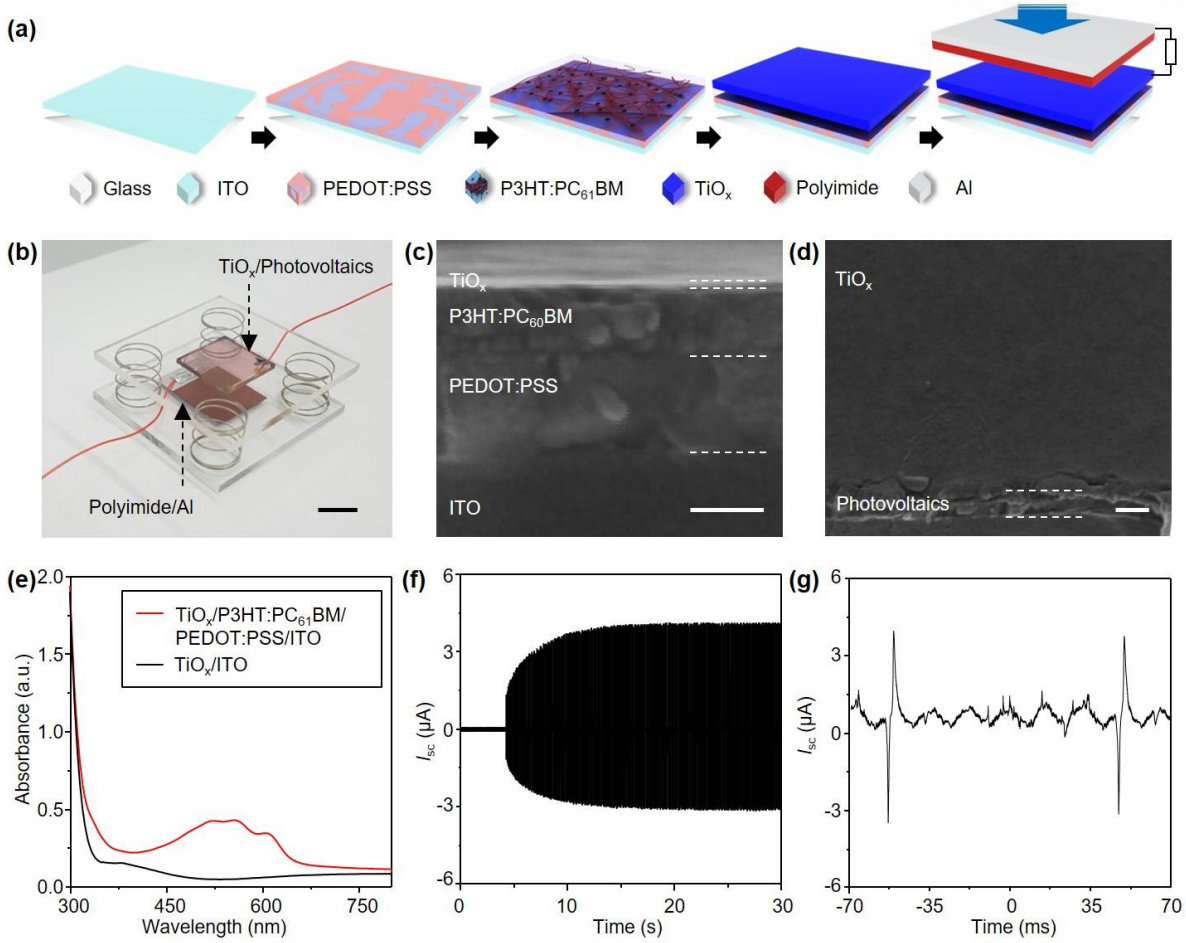

Figure 13. Schematic diagram of the photovoltaic structured triboelectric nanogenerator. (a) schematic illustration for the fabrication process of triboelectric nanogenerator. (b) a photo of triboelectric nanogenerator. (c), (d) cross-sectional and top view (TiO_x) SEM images. (e) the absorption spectra of TiO_x/P3HT:PC_{61}BM/PEDOT:PSS/ITO and TiO_x/ITO layers. (f) the output short-circuit current of the triboelectric nanogenerator with the measuring time under dark condition. (g) the expanded view of the output short-circuit current.

Without the TiO_x layer in Figure 14b, the device shows a typical photovoltaic response, that is, the short-circuit current (I_{sc}) of 8.98 mA/cm^2, the open-circuit voltage (V_{oc}) of 0.60 V, and the fill factor (FF) is 0.63, which are comparable to those reported in previous studies.[16]

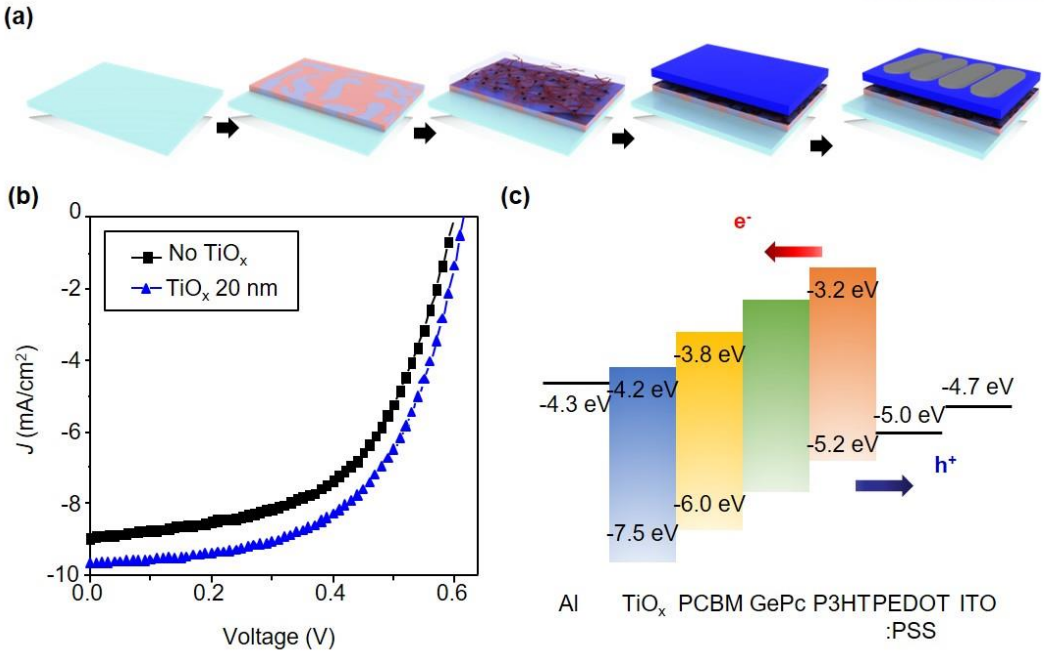

Figure 14. (a) The fabrication process of organic photovoltaic cells with Al/TiO_x/P3HT:$PC_{61}BM$/PEDOT:PSS/ITO/glass. (b) The current-density versus voltage (*J*–*V*) characteristics with and without TiO_x layer. (c) The energy band diagrams for Al/TiO_x/P3HT:$PC_{61}BM$/PEDOT:PSS/ITO/glass under light illumination.

The power conversion efficiency can be calculated to be 3.39 % by using $\eta_e=I_{sc}V_{oc}FF/P_{inc}$, where P_{inc} is the intensity of incident light. Under the open-circuit conditions of steady state illumination, the generation of photo-induced current means that the photogenerated free carriers accumulates at the anode and cathode due to the potential difference between them, as shown in Figure 14c. As the TiO_x layer of approximately 20 nm is deposited on P3HT:$PC_{61}BM$ layer, the I_{sc} and V_{oc} increase to 9.72 mA/cm^2 and 0.62 V, respectively, thus, the η increases to 3.62, corresponding to approximately 6.4 % increase in the efficiency. It is well-known that the main requirements for the electron transport layer (ETL) is a good electron transport property and, when the light is collected through it, transparency to the solar radiation. This limits the choice to a few materials, among which are the well-

known and widely-used ZnO and TiO_x. The amorphous TiO_x ETL layer has been characterized by high electron mobility and high transparency in the visible range. It is possible to realize a TiO_x ETL layer at room temperature from solution without any post-deposition annealing process.[17] As the electrons mainly travel inside the PCBM phase and the holes mainly travel inside the P3HT phase towards the respective electrodes, the inverted configuration is the best one, being characterized by a self-assembled ETL (hole blocking) at the electron extraction electrode, thus increasing the charge extraction efficiency and reducing the bimolecular recombination at the electrodes.

5.3.2 Output performance under dark and light

As mentioned above, the TENG was fabricated by placing the polyimide layer on the TiO_x before the deposition of the Al metals. TiO_x was used as the bottom electrode. The Al film (top electrode) was attached on a polyimide, which were connected through an insulating polymer with double-sided adhesive with a thickness of 0.03 mm, maintaining an air gap, as shown in Figure 13a. Figure 13c shows the output open-circuit voltage of the TENG under a compressive force of 30 N and a frequency of 10 Hz. Initially, the output open-circuit voltage was measured to be approximately 2 V. It then saturates to approximately 4 V and there is no more increase after 10 sec. A continuous contact gradually accumulate the triboelectric charges on both surface, increasing the output short-circuit current with some cycles of contacting collisions. We will use the saturated signals from now, which are compared with others for the accurate experiments. The short-circuit current was carried out under compressive force of 30 N and at an applied frequency of 10 Hz, plotted in Figs. 15a. The TENG has an active area of around 1×1 cm^2. Under dark condition, the saturated output short-circuit current of approximately 4 μA was generated and its performance looks so stable.

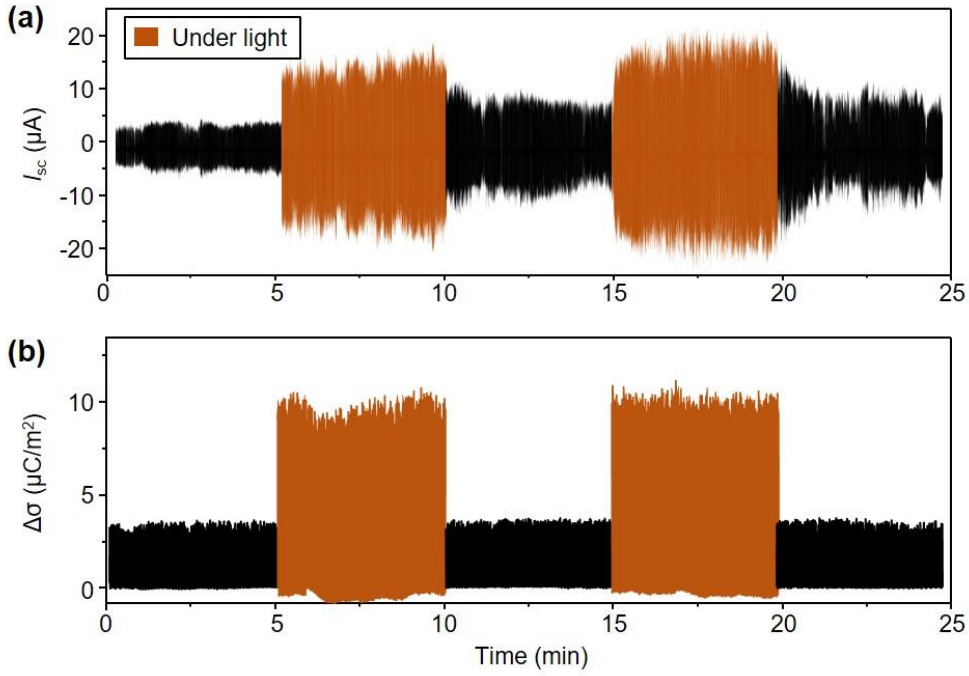

Figure 15. Electrical outputs of triboelectric nanogenerator. (a) the output short-circuit current of the triboelectric nanogenerator under dark condition and white light illumination. (b) the charge density measured under same condition.

When the light is turned on, the output short-circuit current quickly starts to increase and saturates at approximately 15 μA within several seconds. The photo response of the output short-circuit current is quite repeatable although the output short-circuit current in dark condition still increases a little as a function of measuring time. The increase in the output open-circuit voltage and short-circuit current by the light illumination can be clearly observed. We also measured the charge density on the surface of both layers, TiO_x and Polyimide, under dark and light condition, using the electrometer system (Keithley 6514). As shown in Fig. 15b, the charge density was measured to be 4 μC/m^2 and 10 μC/m^2, respectively. This shows that

the enhancement of the output power may ascribe to the increase of the transferred charge density.

5.3.3 TiO_x layer work function variation before and after the light exposure

As one of main factors influencing on the charge density, Kelvin probe force microscope (KPFM) measurements have been carried out aiming at the determining the TiO_x layer work function variation before and after the light exposure, as shown in Figure 16. For the exact measurement, the topography (Fig. 16a) and surface potential (Fig. 16b) of the same region were obtained simultaneously by atomic force microscope (AFM)/KPFM. The topography image reveals very small nanoparticles with characteristic dimensions of approximately 20 nm in size, however, it displays a quite flat surface with an effective roughness less than 10 nm. In a dark condition, the potential maps shows red color over most region although there are a part of the region showing green and blue colors. The work function in the dark condition was determined to be averagely Φ_{dark} = 5.12 eV. With the light exposure on the same position as in the dark, it was changed to blue color although the red color is still visible in the map. This means that the mean work function shifted towards lower values, determined to be $\Phi_{illuminated}$ 4.92 eV. This indicates that by the light illumination, the Fermi level shifted to lower energy by approximately 0.2 eV.

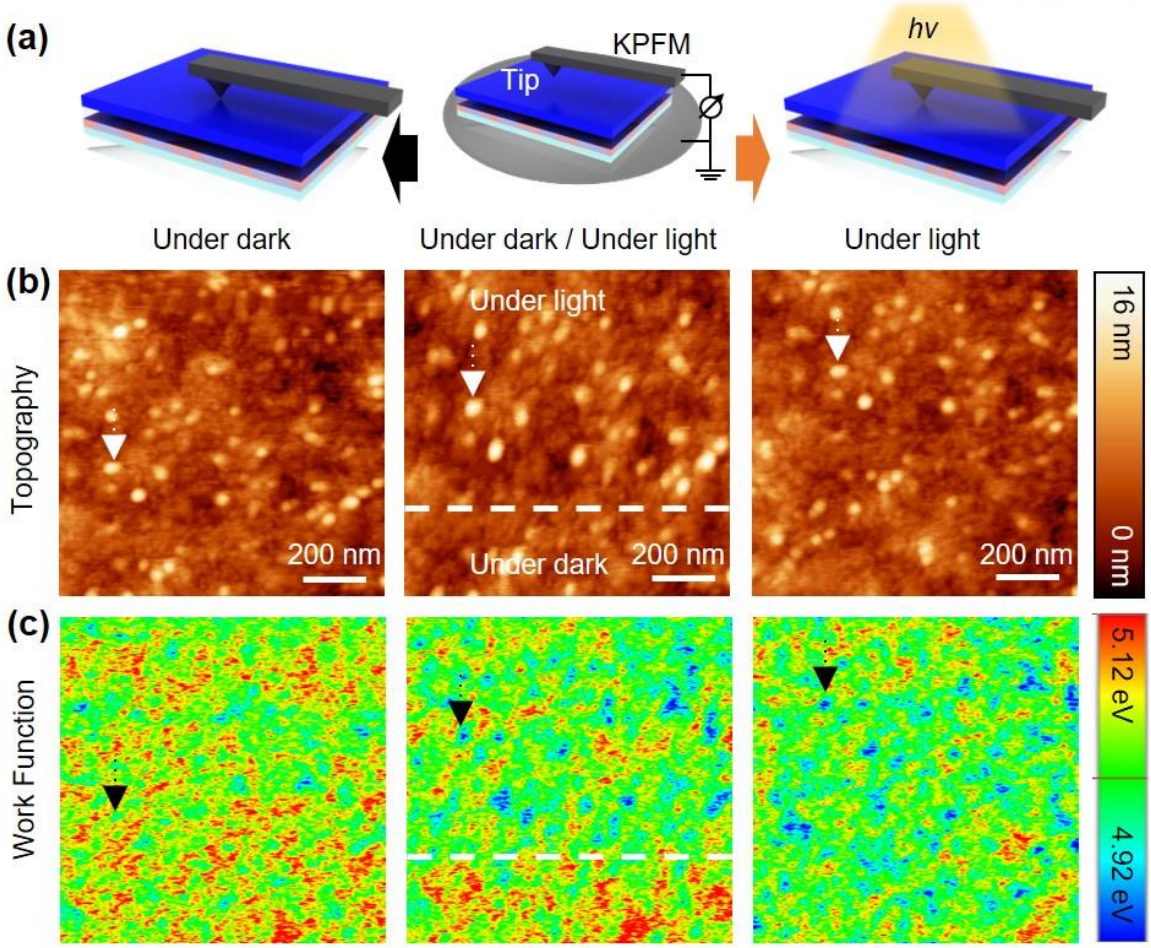

Figure 16. TiO_x layer work function variation before and after the light exposure. (a) the schematic illustration of KPFM measurement under dark condition and light illumination. (b) Topography and (c) surface potential maps of TiO_x layer on P3HT:PC_{61}BM/PEDOT:PSS/ITO substrate of same region with the light illumination.

5.3.4 Effect of electron accumulation on output performance

According to the working principles of the photovoltaic structures, photogenerated electrons will be excited to the lowest unoccupied molecular orbital (LUMO) and leave holes in the highest occupied molecular orbital (HOMO). The carriers are separated and moved in the opposite direction due to the internal electric field generated by the asymmetric potential of the electrodes at both ends or built-in potential of the surface.[17] as seen in Fig. 14c. TiO_x was well-known to collect the photogenerated electrons effectively. Thus, the decrease in the work function may be due to the presence of photo-generated electrons at the TiO_x layer due to the internal electric field. In order to further investigate the effects of the accumulation of the photogenerated electrons at the TiO_x layer on the output performance, the carrier concentration was tuned by depositing TiO_x on the SiO_2/Si substrate with the back gate metal (Au) and by applying the gate voltage in Figure 5a. The output open-circuit voltages of the TENGs were also measured with the gate voltage. It was clearly shown that the output open-circuit voltages increased as the gate voltage increased from + 15 to - 15 V in Figure 17b.

When the negative voltage is applied, positive charges are placed at the interface of TiO_x and SiO_2, inducing negative charges at the (near) surface of the TiO_x. The carrier concentration (n) in TiO_x thin film is defined as,

$$n(x) = \int_{E_{n,0}}^{E_{lim,n}} \sum_{v} g_v \frac{m_{n,v,yz}}{\hbar^2 \pi} \sum_{i} \Theta\left(E - E_{n,i}\right) \left|\psi_{n,i}(x)\right|^2 f_{FD}(E) dE$$

where $m_{n,v}$, v, $\hbar$, $\Theta_{(x)}$, $E_{n,i}$, $\psi_{n,i}(x)$, and f_{FD} are the electron effective mass, the valley index, Dirac's constant, the Heaviside step function, the energy of the electron quasi-bound state, channel wave-function and the Fermi-Dirac distribution.[20]

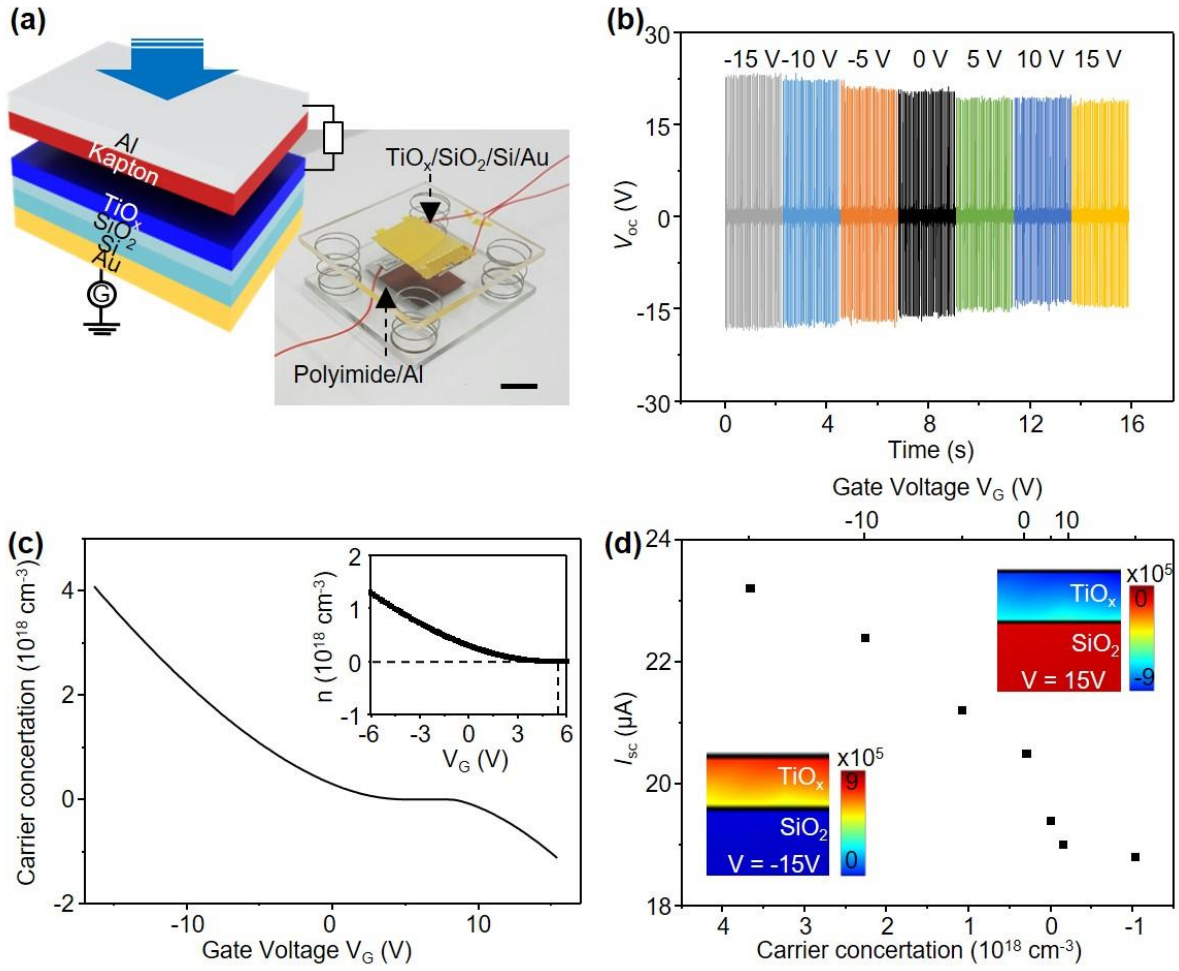

Figure17. Effect of electron accumulation on output performance in TiO_x layer. (a) the schematic picture and a photo of gated triboelectric nanogenerator consisting of the Al/polyimide and $TiO_x/SiO_2/Si/Au$, by having the two physically separated by the springs. (b) the output open-circuit voltage of the triboelectric nanogenerator with the gate voltage. (c) the simulated carrier concentration of the TiO_2 layer on $SiO_2/Si/Au$ substrate. (d) the output short-circuit current of the triboelectric nanogenerator with carrier concentration and gate voltage.

Considering the relative permittivity (130) and bandgap (3.2 eV) of the TiO_2, the carrier concentration with the gate voltage was calculated with MATLAB, plotted in Figure 17c. Here, the thickness of the film was fixed to be 20 nm. At zero gate voltage, the carrier

concentration of the oxide was approximately 2.58 x 10^{17} cm^{-3}. As the gate voltage was varied from – 15 V to 15 V, the carrier concentration decreased and the oxide was changed to p-type from approximately 5 V. The strong gate dependence on the carrier concentration indicates that the output performance will be tuned by the gate voltage.[21] The measured output short-circuit currents with the carrier concentration and the gate voltage was plotted in Figure 17d. As the electron concentration decreased, the output short-circuit current also decreased, indicating that more electrons were transferred to the polyimide at higher negative gate voltage. As the electron concentration decreased to almost 0, the output short-circuit current significantly decreased and there was no more significant decrease when holes become majority carriers. Thus, this result can clearly support that the enhancement mechanism inferred here is due to the accumulation of photogenerated electrons at the TiO_x layer.

To support the above-proposed working mechanism, the COMSOL simulations are performed for the charge density of TiO_x with the gate voltage, as shown in the inset of Figure 17d. The material parameters of the Au, Si, SiO_2 and TiO_2, taken from the COMSOL simulation software, are used for the finite element analysis. The electrical conductivity of Au, Si, SiO_2, and TiO_2 are 4.4 x 10^7, 1.12 x 10^{-12}, 2.83 x 10^{-45}, and 1 × 10^{-9} S/m, respectively. The relative permittivities of the materials are also 6.9, 11.7, 3.9, and 130, respectively. It was clearly seen that as the electron concentration increased, the charge density increased, meaning that the electrons can play as carriers transferred to the polyimide.

According to the previous works, the transferred charge density (σ) on the polyimide surface is defined as

$$\sigma = \frac{[(W - E_0)/e](1 + t/\varepsilon z)}{t/(\varepsilon\varepsilon_0)\ ) + \left(1/\overline{N_s(E)}e^2\right)(1 + t/\varepsilon z)}$$

where W - E_0 is the difference in the effective work functions between two materials, e, t, e, e0, z, and $\overline{N_s(E)}$ are the charge of an electron, distance of space, relative permittivity of polymer, vacuum permittivity of free space, depth of the polyimide film, and the averaged surface density of states.[22] Here, in the dark, the work function of polyimide was measured to be approximately 5.08 eV in Figure 18, which is comparable to those reported in literature.[23]

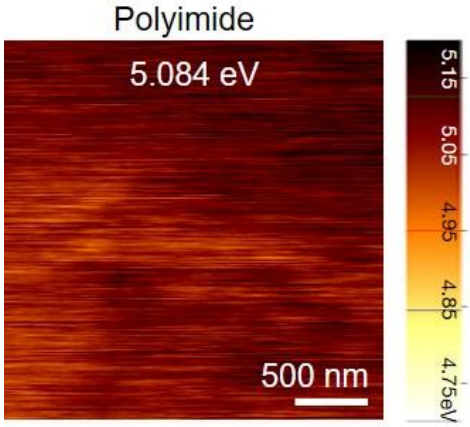

Figure 18. The surface potential map of the polyimide layer under dark condition.

5.3.5 Mechanism of charge transfer

In a dark condition, the Fermi level of TiO_x was represented by a characteristic energy level with an effective work function around 5.12 eV, which is a little higher than the surface energy state of the polyimide. This may imply that the charges will be transferred to the TiO_x from the polyimide until the two energy levels are lined up. However, the charge density generated on the both surface will not be enough for the large output power generation because of the very small work function difference between the two materials. The binding energy of the charges trapped in the polyimide may be quite high, difficult to escape the trapped sites, thereby, resulted in low charge concentration. When the light is illuminated, the negative shift

of the work function of - 0.2 V will lead to the inversion of the charge transfer from the TiO_x to the polyimide and result in an enlarged potential difference between the two materials, which will in turn increase the probability of charge transfer by tunneling upon contact. To support this assumption, we expanded the output signals measured in a dark and lighted condition, plotted in Figure 19a. In a dark condition, when the two materials are released after the pressed, the electrons are flowing from the TiO_x to the top electrode. It indicates that the charges are transferred from the polyimide to TiO_x. With the light illumination, the direction of the electron flow through the external circuit was reversed and the output short-circuit current was enhanced by approximately twice, plotted in Figure 19b. This clearly shows that the more charges are transferred from the TiO_x to the polyimide, in a good agreement with the assumption.

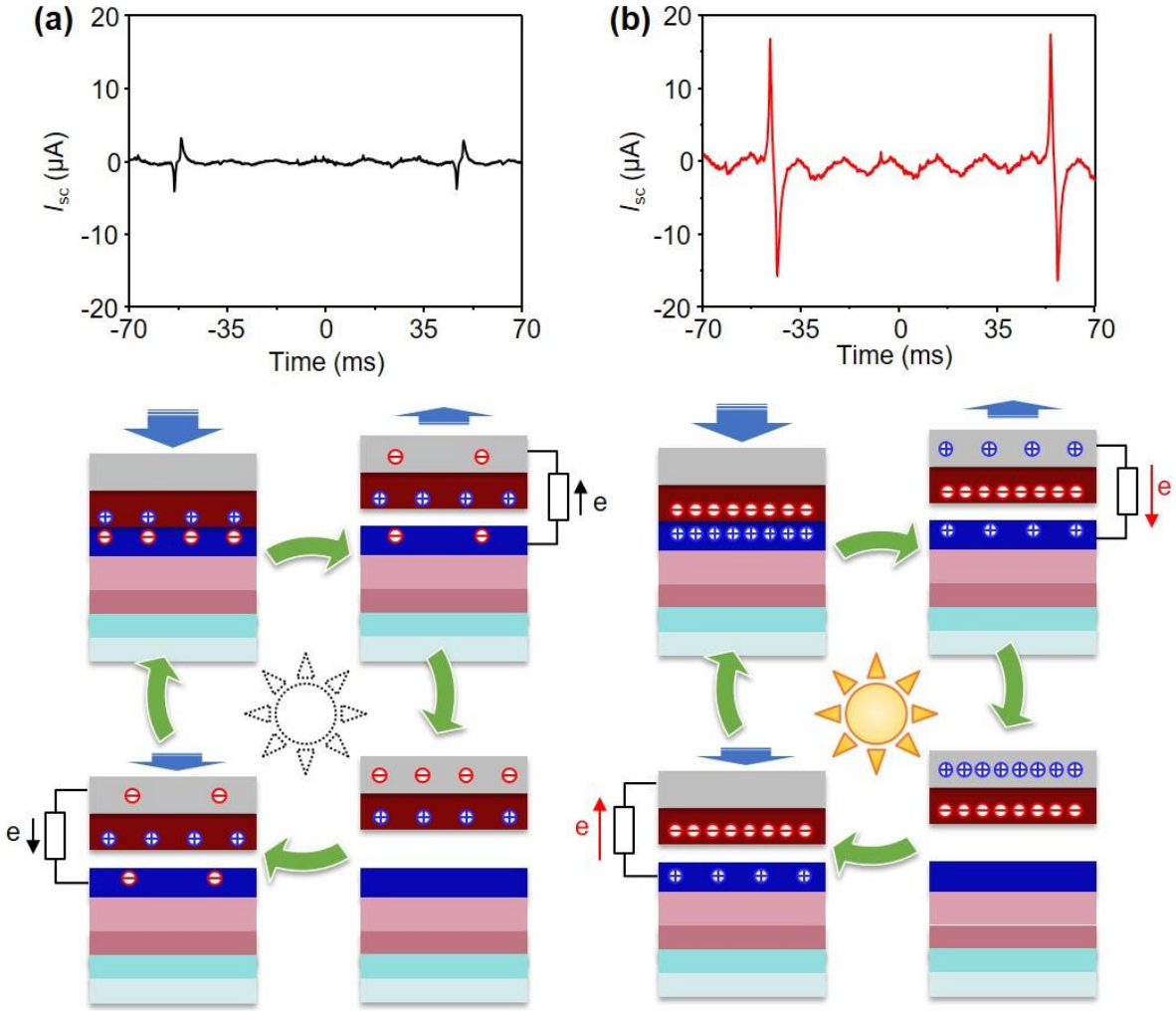

Figure 19. The output short-circuit current of triboelectric nanogenerator consisting of Al/Polyimide/TiO_x/P3HT:PC_{61}BM/PEDOT:PSS/ITO. (a) under dark condition. (b) white light illumination

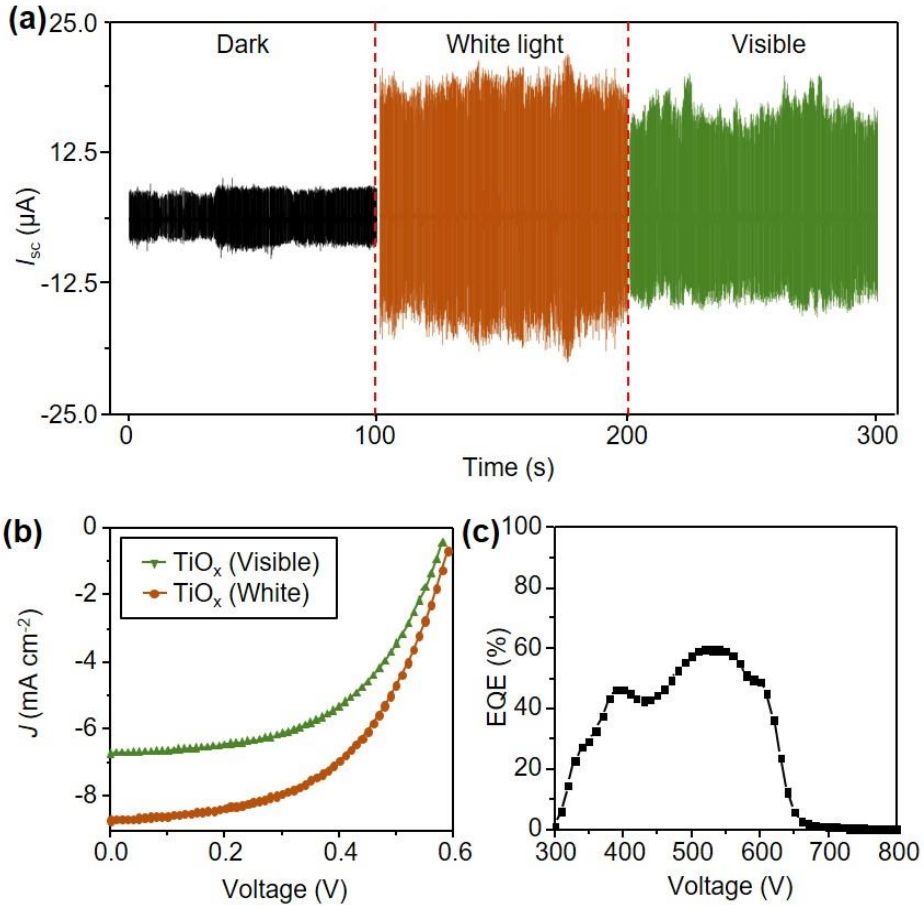

Figure 20. The wavelength-dependent measurement of the electrical output. (a) the output short-circuit current of the triboelectric nanogenerator consisting of Al/Polyimide/TiO_x/P3HT:PC_{61}BM/PEDOT:PSS/ITO with the wavelength of the incident light. (b) the short-circuit current density of the solar cell consisting of Al/TiO_x/P3HT:PC_{61}BM/PEDOT:PSS/ITO with the wavelength of the incident light. (c) the EQE with the wavelength.

5.3.6 Wavelength-dependent measurement

To gain further insight into the enhanced output performance of the TENG, the output signals with the wavelength of the incident light were measured, plotted in Figure 20a. In dark conditions, an output short-circuit current of approximately 4 μA was generated and the output short-circuit current increased up to 20 μA after the white light was illuminated, in a good agreement with the above results. Here, UV light (< 400 nm) was filtered and exposed at the same condition to see the effect of the visible light. The increase in the output short-circuit current were also observed after exposing the sample to the light although there was a little decrease in the short-circuit current. This means that the visible light strongly contributes to the enhancement of the output performance.

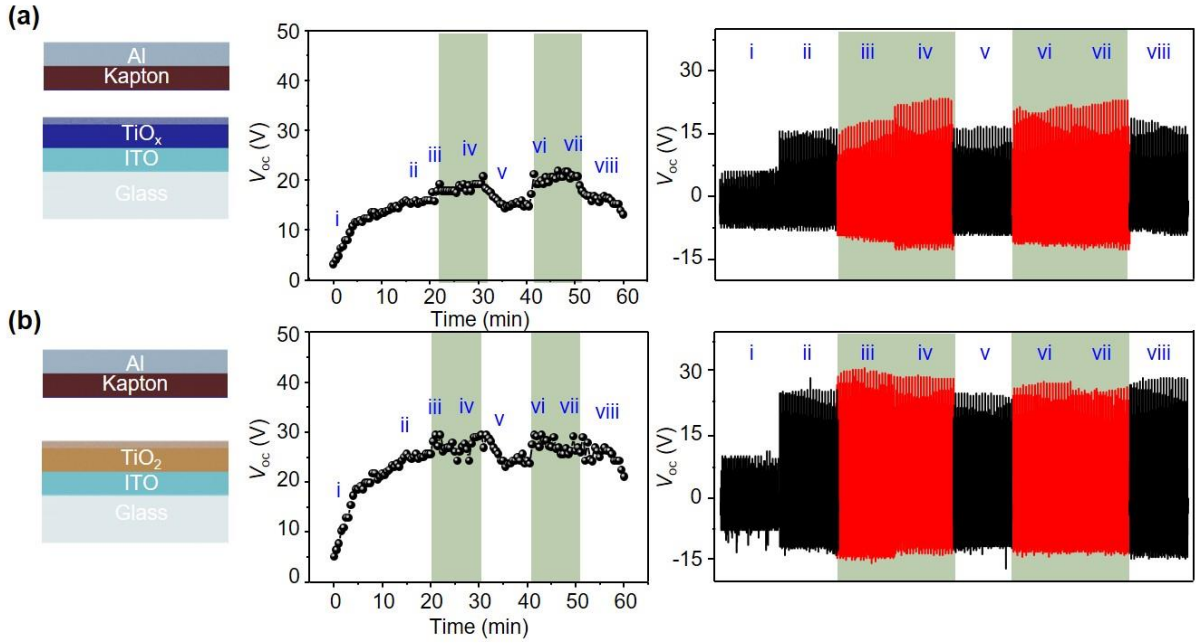

Figure 21. The output open-circuit voltages of the triboelectric nanogenerators consisting of the (a) Al/Polyimide and TiO_x/ITO/glass. (b) Al/Polyimide and TiO_2/ITO/glass with the incident white light.

In general, the UV light promotes the electrons in valence band to the conduction band or the trap states, thereby, the oxide becomes more conductive. This may be quite effective in transferring more electrons to the polyimide film during the physical contact. For further investigation, TiO_x and TiO_2 were directly deposited on ITO/glass substrate and TENGs were fabricated. The white light was illuminated onto both oxides under same conditions and the output open-circuit voltage was measured, plotted in Figure 21. It was clearly shown that there were not significant change in output open-circuit voltages for both TENGs. This may show that the effect of the UV light illumination on the output performance of the TENGs is negligible because the surface potential is not changed via visible light illumination because of the large bandgap energy of the oxides. Actually, as shown in Figure 22, the potential maps of both oxides showed that their values were not significantly changed after exposing the samples to white light although there were a little decrease (< 0.05 eV) in the surface potential.

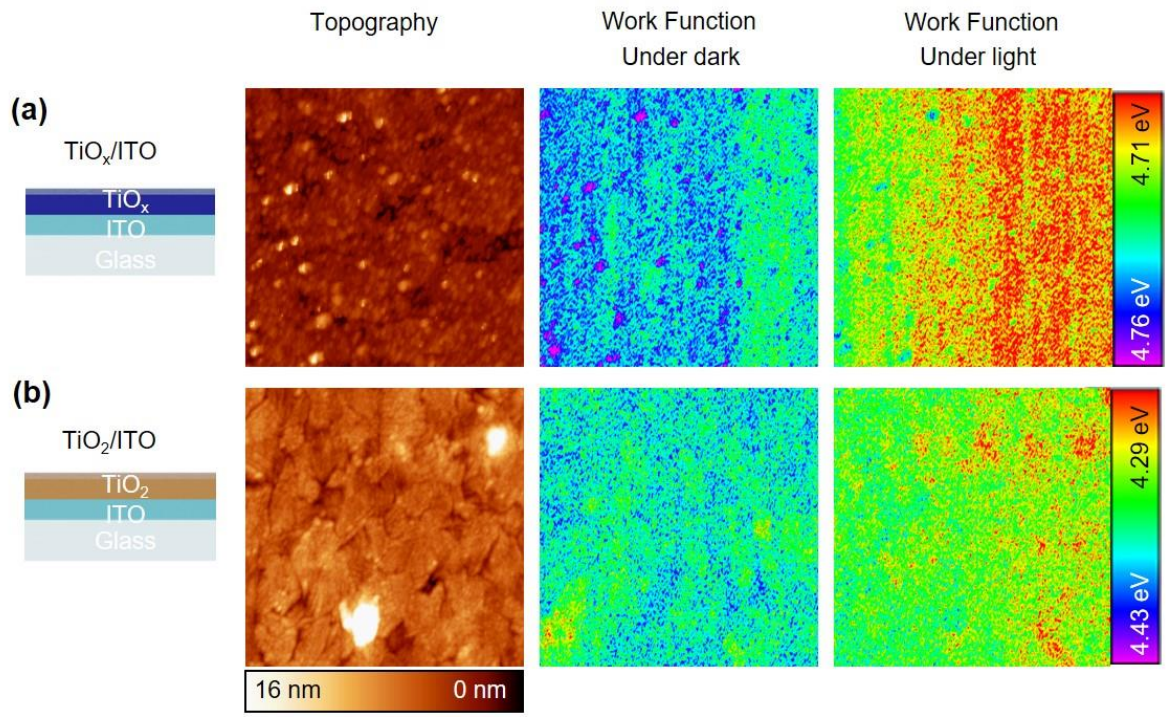

Figure 22. The topography and surface potential maps of (a) TiO_x/ITO/glass and (b) TiO_2/ITO/glass with white light illumination.

We also measured the output performance of the photovoltaic structures (Al/TiO_x/P3HT:$PC_{61}BM$/PEDOT:PSS/ITO/glass) as a function of wavelength in Figure 20b. When UV-filtered light is illuminated, the I_{sc} of 6.9 mA/cm^2 and the V_{oc} of 0.60 V were observed. When white light is illuminated, the I_{sc} increased to 9.8 mA/cm^2, by 40 % enhancement. This may explain the enhancement of the output short-circuit current with the UV light observed in Figure 20a as UV light can assist the transport of the photogenerated electrons to the TiO_x[24-26]. However, the enhancement was not so high due to the low EQE in UV light region, as shown in Figure 20c.[27,28] Also, the electron-hole pairs generated in TiO_x by UV light illumination was known to recombine very quickly (~ 100 ps), while the recombination of the photogenerated electrons transported from the active layer with holes in TiO_x are quite slow (> 200 ps). As a result, it can be concluded that a large amount of photogenerated electrons can be transported to the polyimide layer during the physical contact.[29-31]

Finally, to show that the enhancement of the output power is due to the charge transfer, we performed a series of comparative experiments using X-ray photoelectron spectroscopy (XPS) in Supplementary Fig. 23. After the contact-separation at 10,000 times, the core level spectra of O 1s, C 1s, and Ti 2p were measured. There was no change in binding energy of the O 1s and C 1s peaks, and no additional peak were not observed. In Ti 2p spectra, any Ti element was not observed after the contact-separation. Based on the results, we convince that there is no material transfer between TiO_x and polyimide meaning the power generation may be originated from the charge transfer.

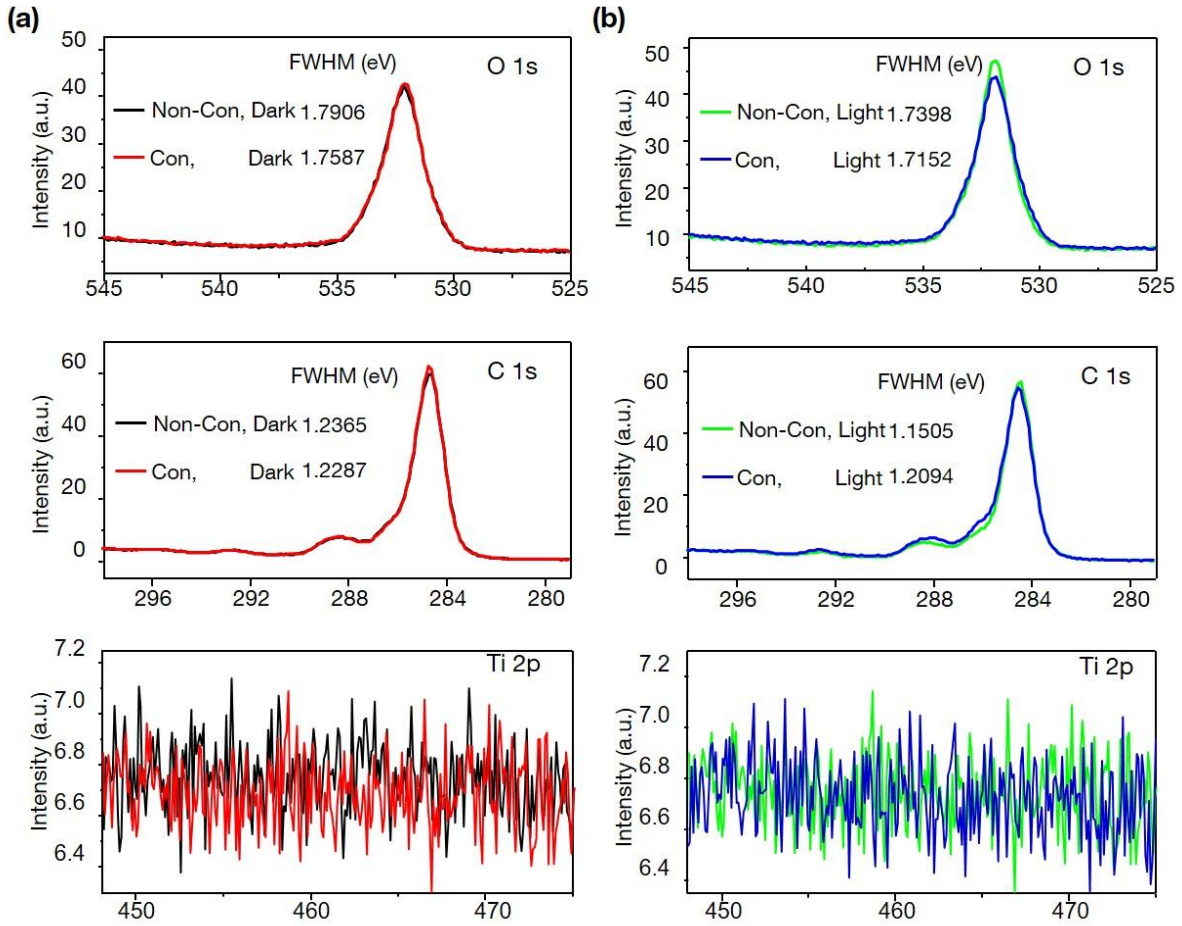

Figure 23. The core level spectra of O 1*s*, C 1*s*, and Ti 2*p* of the TiO_x layer before and after the physical contact under (a) dark condition and (b) light illumination.

5.4 Conclusion

Here, we demonstrated the visible-light-induced unusual inversion in charge transfer and the increase of the tribo-charges transferred across the oxide/polyimide interface during the physical contact, which remarkably enhanced the output performance of the triboelectric nanogenerator. Under light illumination, the surface potential maps of TiO_x layer on P3HT:PC_{61}BM/PEDOT:PSS/ITO substrate showed the significant decrease of the work function by approximately 0.2 eV, positioned to be at lower than that of the polyimide and thus

increasing the work function difference with the polyimide. Therefore, more charges are transferred to the polyimide, increasing the surface charge density on both surface. The wavelength-dependent measurement of the output open-circuit voltages revealed that the photogenerated electrons from active layer via visible light were accumulated at the surface of TiO_x, enhancing the output short-circuit current of the triboelectric nanogenerator by 5 times, supported by the gate voltage-dependent output performance of the nanogenerator with $TiO_x/SiO_2/Si$ substrate connected to the back gate metal. These results can contribute to the designs of the energy harvesting devices with high performance as well as the development of the self-powered selective wavelength photodetectors.

5.5 References

[1] Z-H. Lin, G. Zhu, Y. S. Zhou, Y. Yang, P. Bai, J. Chen, and Z. L. Wang. *Angew. Chem.* **2013**, *125*, 5169.

[2] Z-H. Lin, Y. Xie, Y. Yang, S. Wang, G. Zhu, and Z. L. Wang. *ACS Nano*, **2013**, *7*, 4554.

[3] X. Ma, D. Zhao, M. Xue, H. Wang, T. Cao. *Angew. Chem*. **2010**, *122*, 5669.

[4] D. Zhao, L. Duan, M. Xue, W. Ni, T. Cao. *Angew. Chem*. **2009**, *121*, 6827.

[5] E. S. Polsen, A. G. Stevens, and A. J. Hart. *ACS Appl. Mater. Interfaces*, **2013**, *5*, 3656.

[6] T. Zhou, C. Zhang, C. B. Han, F. R. Fan, W. Tang, and Z. L. Wang. *ACS Appl. Mater. Interfaces*, **2014**, *6*, 14695.

[7] K. N. Kim, J. Chun, J. W. Kim, K. Y. Lee, J-U Park, S-W Kim, Z. L. Wang, and J. M. Baik. *ACS Nano*, **2015**, *9*, 6394.

[8] Y. Zhu, B. Yang, J. Liu, X. Wang, L. Wang, X. Chen, and C. Yang. *Scientific Reports*, **2016**, *6*, 22233.

[9] Q. Zheng, H. Zhang, B. Shi, X. Xue, Z. Liu, Y. Jin, Y. Ma, Y. Zou, X. Wang, Z. An, W. Tang, W. Zhang, F. Yang, Y. Liu, X. Lang, Z. Xu, Z. Li, and Z. L. Wang. *ACS Nano*, **2016**, *10*, 6510.

[10] Y. Zi, J. Wang, S. Wang, S. Li, Z. Wen, H. Guo, and Z. L. Wang. *Nature Communications*, **2016**, *7*, 10987.

[11] L. Dhakar, S. Gudla, X. Shan, Z. Wang, F. E. H. Tay, C-H. Heng, and C. Lee, *Sci Rep.*, **2016**, *6*, 22253.

[12] J. Chun, B. U. Ye, J. W. Lee, D. Choi, C-Y. Kang, S-W. Kim, Z. L. Wang, and J. M. Baik. *Nature Communications*, **2016**, *7*, 12985.

[13] S. Wang, Y. Xie, S. Niu, L. Lin, C. Liu, Y. S. Zhou, and Z. L. Wang. *Adv. Mater.*, **2014**, *26*, 6720.

[14]L. S. McCarty, and G. M. Whitesides. *Angew. Chem.*, **2008**, *47*, 2188.

[15]M. Mirkowska, M. Kratzer, C. Teichert, and H. Flachberger. *BHM*, **2016**, *161*, 359.

[16]J. Li, S. Kim, S. Edington, J. Nedy, S. Cho, K. Lee, A. J. Heeger, M. C. Gupta, and J. T. Yates. *Solar Energy Materials & Solar Cells*, **2011**, *95*, 1123.

[17]S. Lattante. *Electronics*, 2014, *3*, 132.

[18]S. C. Ameta, and R. Ameta. *Springer Berlin Heidelberg*, **2015**, *1*.

[19]S. D. Brotherton, *Springer International Publishing*, **2013**, *1*.

[20]S. M. Sze, K. K. Ng. *Wiley*, **2007**, *3*.

[21]C. A. Richter, A. R. Hefner, and E. M. Vogel. *IEEE ELECTRON DEVICE LETTERS*, **2002**, *22*, 35.

[22]Y. S. Zhou, S. Wang, Y. Yang, G. Zhu, S. Niu, Z-H. Lin, Y. Liu, and Z. L. Wang. *Nano Lett.*, **2014**, *14*, 1567.

[23]K. N. Kim, Y. K. Jung, J. Chun, B. U. Ye, M. Gu, E. Seo, S. Kim, S-W. Kim, B-S. Kim, and J. M. Baik. *Nano Energy*, **2016**, *26*, 360.

[24]T. Kuwabara, H. Sugiyama, T. Yamaguchi, and K. Takahashi. *Thin Solid Films*, **2009**, *517*, 3766.

[25]R. Steim, F. R. Kogler, and C. J. Brabec. J. *Mater. Chem.*, **2010**, *20*, 2499.

[26]Y. Li, J. K. Cooper, W. Liu, C. M. S. Fella, M. Amani, J. W. Beeman, A. Javey, J. W. Ager, Y. Liu, F. M. Toma and I. D. Sharp. *Nature Communications*, **2016**, *7*, 12446.

[27]H. J. Bolink, E. Coronado, A. Forment-Aliaga, M. Lenes, A. L. Rosa, S. Filippone, and N. Martín. *J. Mater. Chem.*, **2011**, *21*, 1382.

[28]M. Ikram, S. Ali, R. Murray, A. Hussain, and S. I. Shah. *Curr. Appl. Phys.*, **2015**, *15*, 48.

[29]Y. Xie, Y. Li, L. Xiao, Q. Qiao, R. Dhakal, Z. Zhang, Q. Gong, D. Galipeau, and X. Yan. *J. Phys. Chem. C*, **2010**, *114*, 14590.

[30]M. Sachs, E. Pastor, A. Kafizas, and J. R. Durrant. *J. Phys. Chem. Lett.*, **2016**, *7*, 3742.

[31] I-W. Hwang, J. Y. Kim, S. Cho, J. Yuen, N. Coates, K. Lee, M. Heeney, I. McCulloch, D. Moses, and A. J. Heeger. *J. Phys. Chem. C*, **2008**, *112*, 7853.

CURRICULUM VITAE OF BYEONG UK YE

I. PROFESSIONAL AFFILIATION AND CONTACT INFORMATION

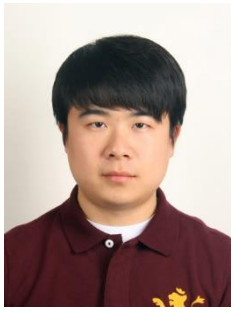

Office Address:

Department of Materials Science and Engineering,

Ulsan National Institute of Science and Technology (UNIST), South Korea

UNIST-gil 50, Eonyang-eup, Ulju-gun, Ulsan, Republic of Korea, 689-798

Tel: +82-52-217-2391, Fax: +82-52-217-2309

E-mail: buye@unist.ac.kr/ buye2391@gmail.com

Homepage: http://unistscml.wixsite.com/jbaiklab

II. SUMMARY OF QUALIFICATIONS

1. Two years' experience model device designing, testing and optimizing nanogenerators
2. Four years' experience manufacturing InGaN based conventional and three-dimensional structures of LED by using MOCVD
3. Three years' experience ZnO Nano-structure grown on heterogeneous surface structures by hydrothermal method
4. Proven ability to work on teams, communicate effectively, and manage projects

III. EDUCATION

B.Sc., 2012, Department of Advanced Materials & System Engineering, Kumoh National Institute of Technology, South Korea.

Combined M.D./Ph. D., 2012~, Department of Materials Science and Engineering, Ulsan National Institute of Science and Technology (UNIST), South Korea.

Major: Material Science and Engineering

Supervisor: Professor, Jeong Min Baik

IV. FIELD EXPERIENCES

Operator, XRS, Pohang Accelerator Laboratory (PAL), 10 Dec. 2013 ~ 11 Dec. 2013

- In-situ synchrotron radiation diffraction of self-guided growth in vanadium oxide nanowires

Operator, XRS KIST-PAL, Pohang Accelerator Laboratory (PAL), 9 Apr. 2012 ~ 10 Apr. 2012

- Crystallinity variation of piezoelectric hemispheres under tensile stress

Researcher, Materials Science and Engineering, Ulsan National Institute of Science and Technology (UNIST), Jul. 2010 ~ Nov. 2012

- Design and fabrication of InGaN LED
- ZnO Nano-structure grown on heterogeneous surface structures by hydrothermal method

V. SKILLS

1. Equipment: Sputter, E-beam evaporator, 6×2" Showerhead-type MOCVD, CVD, RIE, Asher, HR-XRD, SEM, XRS (Pohang Accelerator Laboratory), Photolithographic Aligner, Oscilloscope, Photoluminescence Spectroscopy, Nanovoltmeter, Picoammeter, Electrometer, Sourcemeter, Switch/multimeter
2. Technical: Auto CAD, 3D MAX, Rhino, TEM analysis

VI. HONORS:

2014	The Award of Excellence in the Academic Division of Materials Photo Contest (KIMM), 2014
2011	Best Poster Award in the Korean Institute of Chemical Engineers (KIChE) Spring Conference, 2011

VII. PUBLICATION LIST:

1. **Byeong Uk Ye**, Sangyun Lee, Minbok Jeong, Jinsung Chun, Jin Woong Kim, Hyung-Joon Shin, Myoung Hoon Song and Jeong Min Baik, "Visible-light-induced Unusual Inversion in Charge Transfer and Increase of the Tribo-charges at the oxide/polyimide interface", In preparation (2016)

2. **Byeong Uk Ye,** Jae Won Lee, Kyeong Nam Kim, Jin Pyo Lee, and Jeong Min Baik, "Toward 1 mA/cm^2 Output Current in Triboelectric Nanogenerator", In preparation (2016)

3. Jae Won Lee, **Byeong Uk Ye**, Kyeong Nam Kim, Hyojin Kang, Changduk Yang, Jeong Min Baik, “PVDF-Graft based Triboelectric Nanogenerator as Effective Dielectrics”, In preparation (2016)

4. Jinsung Chun, **Byeong Uk Ye**, Jae Won Lee, Chong-Yun Kang, Dukhyun Choi, Sang-Woo Kim, Zhong Lin Wang, Jeong Min Baik, “Boosted Output Performance of Triboelectric Nanogenerator via Electric Double Layer Effect”, *Nature Communications*, 2016, 7, 12985. IF = 11.329

5. Hee Jun Kim, Joonmo Park, **Byeong Uk Ye**, Chul Jong Yoo, Jong-Lam Lee, Sang-Wan Ryu, Heon Lee, Kyoung Jin Choi*, and Jeong Min Baik, "Parallel Aligned Mesopore Arrays in Pyramidal-Shaped Gallium Nitride and Their Photocatalytic Applications", *ACS Appl. Mater. Interfaces*, 2016, 28, 18201–18207. IF = 7.145

6. Kyeong Nam Kim, Yun Kyung Jung, Jinsung Chun, **Byeong Uk Ye**, Minsu Gu, Eunyong Seo, Seongsu Kim, Sang-Woo Kim, Byeong-Su Kim*, Jeong Min Baik, "Surface dipole enhanced instantaneous charge pair generation in triboelectric nanogenerator", *Nano Energy*, 2016, 26. 360-370. IF = 11.553

7. **Byeong Uk Ye**, Byoung.-Joon Kim, Jungho Ryu, Joo Yul Lee, Jeong Min Baik and Kihyon, “Electrospun Ion Gel Nanofibers for Flexible Triboelectric Nanogenerator: Electrochemical Effect on Output Power”, *Nanoscale*, 2015, 7, 16189-16194. IF = 7.76

8. **Byeong Uk Ye***, Ji-Hyun Kim*, Joonmo Park, Chul Jong Yoo, Buem Joon Kim, Hu Young Jeong, Jin-Hoe Hur, Jong Kyu Kim, Jong-Lam Lee and Jeong Min Baik, “Visible Color Tunable Emission in Three-dimensional Light Emitting Diodes by MgO Passivation of Pyramid Tip”, *ACS Appl. Mater. Interfaces,* 2015, 7, 27743-27748. IF = 7.145 *** Equal contribution**

9. Joonmo Park, Jae Won Lee, **Byeong Uk Ye**, Sung He Chun, Sang Hoon Joo, Hyunwoong Park, Heon Lee, Hu Young Jeong, Myung Hwa Kim and Jeong Min Baik, "Structural Evolution of Chemically-Driven RuO_2 Nanowires and 3-Dimensional Design for Photo-Catalytic Applications", *Sci. Rep.*, 2015, 5, 11933. IF = 5.578

10. Songyi Lee, Yukyung Cho, **Byeong Uk Ye**, Jeong Min Baik, Myung Hwa Kim and Juyoung Yoon, "Unprecedented colorimetric responses of polydiacetylenes driven by plasma induced polymerization and their patterning applications" *Chem. Commun*., 2014, 50, 12447-12449. IF = 6.834

11. Jae Won Lee, **Byeong Uk Ye**, Dong-Yeong Kim, Jong Kyu Kim, Jong Heo, Hu Young Jeong, Myung Hwa Kim, Won Jun Choi, and Jeong Min Baik, "ZnO Nanowire-Based Antireflective Coatings with Double-Nanotextured Surfaces", *ACS Appl. Mater. Interfaces*, 2014, 6, 1375-1379. IF = 7.145

12. **Byeong Uk Ye**, Buem Joon Kim, Joonmo Park, Hu Young Jeong, Jae Yong Park, Jong Kyu Kim, Jin-Hoe Hur, Myung Hwa Kim, Jong-Lam Lee, and Jeong Min Baik, "Three-dimensional Branched Nanowire Heterostructures as Efficient Light-Extraction Layer in Light-Emitting Diodes", *Adv. Funct. Mater*. 2014, 24, 3384-3391. IF = 11.805

13. **Byeong Uk Ye**, Buem Joon Kim, Yang Hee Song, Jun Ho Son, Hak ki Yu, Myung Hwa Kim, Jong-Lam Lee, and Jeong Min Baik, "Enhancing Light Emission of Nanostructured Vertical Light-Emitting Diodes by Minimizing Total Internal Reflection", *Adv. Funct. Mater*. 2012, 22, 632-639. IF = 11.805

14. **Byeong Uk Ye**, Hak Ki Yu, Myung Hwa Kim, Jong-Lam Lee, Jeong Min Baik, "Modulating ZnO Nanostructure Arrays on Any Substrates by Nanolevel Structure Control", *J. Phys. Chem. C*, 2011, 115, 7987-7992. IF = 4.722

15. Youmin Lee, **Byeong Uk Ye**, Hak Ki Yu, Jong-Lam Lee, Myung Hwa Kim, and Jeong Min Baik, "Facile Synthesis of Single Crystalline Metallic RuO_2 nanowires and Electromigration-Induced Transport Properties", *J. Phys. Chem. C*, 2011, 115, 4611-4615. IF = 4.722

VIII. PATENTS

1. Byeong Uk Ye et al, TRIBOELECTRIC GNERATOR, 10-2016-0057136 (2016)
2. Byeong Uk Ye et al, TRIBOELECTRIC GNERATOR, 10-2016-0057217 (2016)
3. Byeong Uk Ye et al, TRIBOELECTRIC GNERATOR, 10-2016-0057218 (2016)
4. Byeong Uk Ye et al, ARTIFICIAL LIGHTNING GENERATOR BASED CHARGE-PUMP AND METHOD THEREOF, 10-2015-0157097 (2015) **PCT: 10-2015-0157097**, **Technology transfer** (Samsung Electronics)
5. Byeong Uk Ye et al, METHOD OF THE PYRAMID-SHAPED LIGHT EMITTING DIODE USING A SELECTIVE ELECTRODE, 10-2015-0020279 (2015)
6. Byeong Uk Ye et al, LIGHT EMITTING DEVICE COMPRISING BRANCHED NANOWIRES HAVING HETEROSTRUCTURE, 10-2014-0011468 (2014)
7. Byeong Uk Ye et al, LIGHT-EMITTING DIODES WITH NANOWIRE HETEROSTRUCTURES OF THREE-DIMENSIONAL BRANCHED FABRICATION AND MANUFACTURING METHOD THEREOF, 10-2014-0011105 (2014)
8. Byeong Uk Ye et al, METHOD FOR MANUFACTURING OF NITRIDE-BASED LED, 10-2013-0006823 (2013), 10-1434318 (2014)
9. Byeong Uk Ye et al, Method For Forming Antireflection Coating Of Solar Cell, 10-2012-0138728 (2012), 10-1363990 (2014)
10. Byeong Uk Ye et al, LIGHT EMITTING DEVICE AND METHOD OF FABRICATING THE SAME, 10-2013-0096330 (2013)

11. Byeong Uk Ye et al, LIGHT EMITTING DIODE DEVICE AND METHOD FOR FABRICATING THE SAME, 10-2012-0046769 (2012), 10-1322927(2013)
12. Byeong Uk Ye et al, Method Of Forming Gallium Nitride Nano Structure Using Nano Sphere, 10-2011-0115572 (2011), 10-1367694 (2014)
13. Byeong Uk Ye et al, METHOD OF MANUFACTURING LIGHT EMITTING DIODE USING ZINC OXIDE NANO-RODS AS A MASK, 10-2010-0139613 (2010)

IX. PRESENTATIONS (INTERNATIONAL CONFERENCE)

1. International Workshop on Piezoelectric Materials and Applications in Actuators & Energy Conversion Materials and Devices (IWPMA & ECMD 2016), Korea, August 21-24. Poster: Charge Enhancing Mechanism in Solar-Assisted Triboelectric Nanogenerator.
2. Nanoenergy and Nanosystems (NENS 2016), China, July 13-15, 2016. **Oral presentation**: Solar Enhanced Triboelectric Nanogenerator Performance and Unusual Inversion in Charge Transfer.
3. Materials Challenges in Alternative & Renewable Energy (MCARE 2016), USA, April 17-20, 2016. Poster: Enhanced Triboelectric Nanogenerators based on the stretchable electrode.
4. International Conference on Advanced Electromaterials (ICAE 2015), Korea, November 17-20, 2015. Poster: Visible Color Tunable Emission in Three-dimensional Light Emitting Diodes by MgO Passivation of Ultra-Sharp Pyramid Tip.
5. 2015 MRS Spring Meeting & Exhibit, USA, April 6-10, 2015. **Oral presentation**: Enhanced Triboelectric Nanogenerators based on the selective charge injection.
6. 2014 MRS Spring Meeting & Exhibit, USA, April 21-25, 2014. Poster: Polarization De

pendence of Electroluminescence Properties and Output Voltage in Flexible N-Fac e *p*-GaN Thin Films.

7. International Conference on Advanced Electromaterials (ICAE 2013), Korea, November 12-17, 2012. **Oral presentation**: Three-dimensional Branched Nanowire Heterostructures as Efficient Light-Extraction Layer in Light-Emitting Diodes.
8. International Workshop on Nitride Semiconductors (IWN 2012), Japan, October 14-19, 2012. Poster: Enhancing Light Emission of Nanostructured Vertical Light-Emitting Diodes by Minimizing Total Internal Reflection .
9. International Conference on Metal Organic Vapor Phase Epitaxy (ICMOVPE 2012), Korea, May 20-25, 2012. Poster: Epitaxial Growth of InGaN Nanowire Arrays on Hydrothermally Grown ZnO Substrates for Wafer Scalable Nanostructured Light Emitting Diodes.
10. International Conference on Electronic Materials and Nanotechnology for Green Environment 2010 (ENGE 2010), Korea, November 21-24, 2010. Poster: Patterned growth of a vertically well-aligned ZnO nanorods for tunable light extraction in VLEDs.

IX. PRESENTATIONS (INTERNATIONAL CONFERENCE)

1. 10th Energy Haresting Workshop, USA, September 13-16, 2015. **Oral presentation**: Mesoporous Pores Impregnated with Au Nanoparticles as Effective Dielectrics for Enhancing Triboelectric Nanogenerator Performance under Harsh Environment.
2. Materials Challenges in Alternative & Renewable Energy (MACRE 2015), Korea, February 24-27, 2015. Poster: Mesoporous Pores Impregnated with Au Nanoparticles as Effective Dielectrics for Enhancing Triboelectric Nanogenerator Performance under Harsh Environment.

3. Nanoenergy and Nanosystems 2014 (NENS 2014), China, December 8-10, 2014. **Oral presentation**: Au Nanoparticles-embedded Mesoporous Triboelectric Nanogenerators for Enhanced Surface Charges.
4. International Conference on Electronic Materials and Nanotechnology for Green Environment 2014 (ENGE 2014), Korea, November 16-19, 2014. Poster: Hydrophobic Sponge Structure-Based Triboelectric Nanogenerator.
5. International Nanophotonics and Nanoenergy Conference (INPEC) 2014, Korea, July 1-3, 2014. Poster: Hydrophobic Sponge Structure-Based Triboelectric Nanogenerator.
6. 2nd International Conference on Nanogenerators and Piezotronics (NGPT 2014), USA, June 9-11, 2014. Poster: Hydrophobic Sponge Structure-Based Triboelectric Nanogenerator.
7. 2014 MRS Spring Meeting & Exhibit, USA, April 21-25, 2014. Poster: Hydrophobic Sponge Structure-Based Triboelectric Nanogenerator.
8. 2013 MRS Spring Meeting & Exhibit, USA, April 1-5, 2013. **Oral presentation**: Embossed Thin Films with Hollow Hemispheres for Strain Sensors and Nanogenerators.